Elsevier Editorial System(tm) for Lithos
Manuscript Draft

Manuscript Number: LITHOS8093

Title: Evidence of subduction-related components in sapphirine-bearing gabbroic dykes (Finero Phlogopite Peridotite): Insights into the mantle sources of the Triassic-Jurassic magmatism at the Europe-Africa-boundary

Article Type: VSI:EMAW- Mantle Paradigms

Keywords: sapphirine; Finero; mantle peridotite; dykes; Ivrea Verbano

Corresponding Author: Professor Maurizio Mazzucchelli, Full Professor

Corresponding Author's Institution: Università di Modena e Reggio Emilia

First Author: Tommaso Giovanardi

Order of Authors: Tommaso Giovanardi; Alberto Zanetti; Luigi Dallai; Tomoaki Morishita; Christophe Hémond; Maurizio Mazzucchelli, Full Professor

Abstract: A gabbroic dyke swarm containing magmatic sapphirine occurs in the mantle Finero Phlogopite Peridotite (Ivrea-Verbano Zone, IVZ; Southern Alps). Sapphirine is associated to a peculiar mineral assemblage, including plagioclase, titanian pargasite, titanian phlogopite and apatite: the latter is rich in Cl and calcite inclusions. The dykes i) cut at high angle the mantle foliation, ii) are bounded by orthopyroxenite layers (Opx-Zone), and iii) show a symmetric internal banding, represented by two, outer hornblendite selvages and an inner leucogabbro layer. The sapphirine occurs, along with Al-rich amphibole (locally, close to sadaganaite composition) and green spinel, in mm-thick irregular patches in both the hornblendite salvages.
Major and trace elements of minerals and bulk rock, as well as the isotope O, Sr and Nd composition of minerals, have been investigated for dykes and host peridotite of two different FPP areas.
The melt migration early developed by porous-flow within cm-thick channels, being characterised orthopyroxene-dissolution. With the progression of percolation and reaction, the melt became silica-saturated and an orthopyroxenite layer was segregated in the centre of the channels. Three different evolution stages, involving opening and enlargement of the conduits, determined the layered internal structure of the dykes. The sapphirine and green spinel segregation took place at T> 1000°C in presence of a melt with transient composition, which interstitially migrated and reacted with the cumulus minerals forming the hornblendite layers. Composition of newly-formed amphiboles indicates that the sapphirine parent melt was Al-rich, depleted to strongly depleted in Hf, Zr, Nb, Ta, Ti, Sc, V, MREE and HREE, and characterised by positive Eu anomaly and $(Zr/Hf)_N$ <1. These observations suggest the presence in the transient melt of significant amounts of plagioclase component. Plagioclase assimilation was not observed in the studied veins: it is thus argued that the addition of plagioclase component occurred in hidden magmatic bodies or in the melt source.
The $\delta^{18}O$ of vein amphiboles and plagioclase varies from 6.9 to 8.6‰ SMOW, being well above the mantle range, also taking into account fractionation

upon cooling. The additional observation that the orthopyroxene from the wall, reactive orthopyroxenites has "normal "mantle δ18O values (5.8‰) brings us to conclude that reaction with the host, metasomatised peridotite was not apparently responsible for the heavy isotope O composition argued for parent melt of the dyke minerals: the latter must have been imparted by crustal components sitting at deeper mantle depths. This finding evidences as the Northern IVZ records an extremely prolonged release (lasted from the Variscan orogenic cycle to the Mesozoic exhumation of lithospheric mantle at shallower levels) of K-H2O-rich mantle-derived melts polluted by subduction-related components, placing valuable insight into the comprehension of the Triassic-Jurassic magmatism and the geodynamic environment at the Europe-Africa boundary.

A gabbroic dyke swarm containing magmatic sapphirine occurs in the mantle Finero Phlogopite Peridotite (Ivrea-Verbano Zone, IVZ; Southern Alps). Sapphirine is associated to a peculiar mineral assemblage, including plagioclase, titanian pargasite, titanian phlogopite and apatite: the latter is rich in Cl and calcite inclusions. The dykes i) cut at high angle the mantle foliation, ii) are bounded by orthopyroxenite layers (Opx-Zone), and iii) show a symmetric internal banding, represented by two, outer hornblendite selvages and an inner leucogabbro layer. The sapphirine occurs, along with Al-rich amphibole (locally, close to sadaganaite composition) and green spinel, in mm-thick irregular patches in both the hornblendite salvages.

Major and trace elements of minerals and bulk rock, as well as the isotope O, Sr and Nd composition of minerals, have been investigated for dykes and host peridotite of two different FPP areas.

The melt migration early developed by porous-flow within cm-thick channels, being characterised orthopyroxene-dissolution. With the progression of percolation and reaction, the melt became silica-saturated and an orthopyroxenite layer was segregated in the centre of the channels. Three different evolution stages, involving opening and enlargement of the conduits, determined the layered internal structure of the dykes. The sapphirine and green spinel segregation took place at T> 1000°C in presence of a melt with transient composition, which interstitially migrated and reacted with the cumulus minerals forming the hornblendite layers. Composition of newly-formed amphiboles indicates that the sapphirine parent melt was Al-rich, depleted to strongly depleted in Hf, Zr, Nb, Ta, Ti, Sc, V, MREE and HREE, and characterised by positive Eu anomaly and $(Zr/Hf)_N$ <1. These observations suggest the presence in the transient melt of significant amounts of plagioclase component. Plagioclase assimilation was not observed in the studied veins: it is thus argued that the addition of plagioclase component occurred in hidden magmatic bodies or in the melt source.

The $\delta^{18}O$ of vein amphiboles and plagioclase varies from 6.9 to 8.6‰ SMOW, being well above the mantle range, also taking into account fractionation upon cooling. The additional observation that

the orthopyroxene from the wall, reactive orthopyroxenites has “normal “mantle $\delta^{18}O$ values (5.8‰) brings us to conclude that reaction with the host, metasomatised peridotite was not apparently responsible for the heavy isotope O composition argued for parent melt of the dyke minerals: the latter must have been imparted by crustal components sitting at deeper mantle depths. This finding evidences as the Northern IVZ records an extremely prolonged release (lasted from the Variscan orogenic cycle to the Mesozoic exhumation of lithospheric mantle at shallower levels) of K-H_2O-rich mantle-derived melts polluted by subduction-related components, placing valuable insight into the comprehension of the Triassic-Jurassic magmatism and the geodynamic environment at the Europe-Africa boundary.

***Highlights (for review)**

- Mesozoic Spr-bearing gabbroic dykes with continental crustal components
- Reaction between dyke melts and the metasomatised host enhanced the crustal signature
- The large Al content of the parent melt caused the segregation of magmatic sapphirine
- Dykes record Triassic K-rich Calk-Alkaline to Shosonitic magmatism in Southern Alps

Evidence of subduction-related components in sapphirine-bearing gabbroic dykes (Finero Phlogopite Peridotite): Insights into the mantle sources of the Triassic-Jurassic magmatism at the Europe-Africa-boundary

Tommaso Giovanardi[1,2#], Alberto Zanetti[3#], Luigi Dallai[4], Tomoaki Morishita[5], Christophe Hémond[6], Maurizio Mazzucchelli[2]*

[1]DIPARTIMENTO DI SCIENZE DELLA TERRA E DELL'AMBIENTE, UNIVERSITA' DEGLI STUDI DI PAVIA, VIA FERRATA 1, 27100 PAVIA, ITALY

[2]DIPARTIMENTO DI SCIENZE CHIMICHE E GEOLOGICHE, UNIVERSITA' DEGLI STUDI DI MODENA E REGGIO EMILIA, VIA CAMPI 103, 41121 MODENA, ITALY

[3]ISTITUTO DI GEOSCIENZE E GEORISORSE-C.N.R. PAVIA, VIA FERRATA 1, 27100 PAVIA, ITALY

[4]ISTITUTO DI GEOSCIENZE E GEORISORSE-C.N.R. PISA, VIA MORUZZI 1, 56124 PISA, ITALY

[5]FRONTIER SCIENCE ORGANIZATION, KANAZAWA UNIVERSITY, 920-1192 KANAZAWA, JAPAN

[6]LABORATOIRE GÉOSCIENCES OCÉAN, UMR6538, INSTITUT UNIVERSITAIRE EUROPÉEN DE LA MER, UNIVERSITÉ DE BREST & CNRS, PLACE NICOLAS COPERNIC, F-29280, PLOUZANÉ, FRANCE.

# these authors are equal first authors of this work

* Corresponding author: maurizio.mazzucchelli@unimore.it

Keywords: sapphirine; Finero; mantle peridotite; dykes; Ivrea Verbano

Abstract

A gabbroic dyke swarm containing magmatic sapphirine occurs in the mantle Finero Phlogopite Peridotite (Ivrea-Verbano Zone, IVZ; Southern Alps). Sapphirine is associated to a peculiar mineral assemblage, including plagioclase, titanian pargasite, titanian phlogopite and apatite: the latter is rich in Cl and calcite inclusions. The dykes i) cut at high angle the mantle foliation, ii) are bounded by orthopyroxenite layers (Opx-Zone), and iii) show a symmetric internal banding, represented by two, outer hornblendite selvages and an inner leucogabbro layer. The sapphirine occurs, along with Al-rich amphibole (locally, close to sadaganaite composition) and green spinel, in mm-thick irregular patches in both the hornblendite salvages.

Major and trace elements of minerals and bulk rock, as well as the isotope O, Sr and Nd composition of minerals, have been investigated for dykes and host peridotite of two different FPP areas.

The melt migration early developed by porous-flow within cm-thick channels, being characterised orthopyroxene-dissolution. With the progression of percolation and reaction, the melt became silica-saturated and an orthopyroxenite layer was segregated in the centre of the channels. Three different evolution stages, involving opening and enlargement of the conduits, determined the layered internal structure of the dykes. The sapphirine and green spinel segregation took place at T> 1000°C in presence of a melt with transient composition, which interstitially migrated and reacted with the cumulus minerals forming the hornblendite layers. Composition of newly-formed amphiboles indicates that the sapphirine parent melt was Al-rich, depleted to strongly depleted in Hf, Zr, Nb, Ta, Ti, Sc, V, MREE and HREE, and characterised by positive Eu anomaly and $(Zr/Hf)_N$ <1. These observations suggest the presence in the transient melt of significant amounts of plagioclase component. Plagioclase assimilation was not observed in the studied veins: it is thus argued that the addition of plagioclase component occurred in hidden magmatic bodies or in the melt source.

The $\delta^{18}O$ of vein amphiboles and plagioclase varies from 6.9 to 8.6‰ SMOW, being well above the mantle range, also taking into account fractionation upon cooling. The additional observation that the orthopyroxene from the wall, reactive orthopyroxenites has "normal "mantle $\delta^{18}O$ values (5.8‰) brings us to conclude that reaction with the host, metasomatised peridotite was not apparently responsible for the heavy isotope O composition argued for parent melt of the dyke minerals: the latter must have been imparted by crustal components sitting at deeper mantle depths. This finding evidences as the Northern IVZ records an extremely prolonged release (lasted from the Variscan orogenic cycle to the Mesozoic exhumation of lithospheric mantle at shallower levels) of K-H_2O-rich mantle-derived melts polluted by subduction-related components, placing valuable insight into the comprehension of the Triassic-Jurassic magmatism and the geodynamic environment at the Europe-Africa boundary.

Introduction

It is well-known that subcontinental lithospheric mantle (SCLM) may record significant heterogeneities in terms of both lithologies and geochemical composition as a result of the development of different tectono-magmatic events over a large time span (Mukasa and Shervais, 1999; Rivalenti et al., 2007a,b; Mazzucchelli et al., 2009; 2010; 2016; Borghini et al. 2017; Princivalle et al., 2014; Ponce et al. 2015; Rocco et al., 2017). On the other hand, the petrochemical record on both lithospheric mantle and uprising melts can be very different owing to the geochemical affinity of the melt, the composition of the peridotite mantle column, the modalities of melt migration and the P, T, fO2 and fH2 conditions of the system. A unique study case in which to characterize peculiar modifications affecting uprising mantle melts is the Phlogopite Peridotite mantle unit of Finero (Cawthorn, 1975; Siena & Coltorti, 1989). The Finero Phlogopite-Peridotite (FPP hereafter) is one of the most studied mantle massifs on the Earth. It crops out in the northernmost part of the Ivrea-Verbano Zone (IVZ, western Alps, Italy; Fig. 1) and mainly consists

of an association formed by Phlogopite-bearing Amphibole harzburgites and dunites, both locally associated to Phlogopite-bearing Amphibole pyroxenites. Such a lithologic association is apparently the result of a main episode of pervasive to channelled porous flow migration of melts containing large volume of crustal components, which induced a virtually complete metasomatic recrystallization (Cawthorn, 1975; Siena & Coltorti, 1989 Hartmann & Wedepohl, 1993; Zanetti et al., 1999, 2016; Grieco et al., 2001, 2004; Morishita et al., 2003, 2008; Raffone et al., 2006; Selverstone & Sharp, 2011; Mazzucchelli et al., 2014; Tommasi et al., 2017).

The available geochronological data indicate that main events of melt migration took place in Paleozoic times (Zanetti et al., 2016; Malitch et al., 2017), but many field, petrochemical and geochronological data points to the development of tectono-magmatic events in Mesozoic times (Stähle et al., 1990, 2001; Grieco et al., 2001; Matsumoto et al., 2005; Morishita et al., 2003, 2008; Zanetti et al., 1999; 2016; Malitch et al., 2017).

Giovanardi et al. (2013) studied the occurrence of late Sapphirine-bearing (Spr) gabbroic dykelet swarm previously reported in literature by Siena & Coltorti (1989) and discovered by M. Mazzucchelli. On the basis of a detailed survey of petrography and the major element mineral compositions, they furnish evidence for a multi-stage dyke formation, which involved fractional crystallization associated to different patterns of melt-rocks interactions.

With the aim of better constraining the nature of the primitive melt and the petrological processes inducing the segregation of Spr in the dykes, new, detailed petrochemical data are here reported for dykes and host peridotites close to the area studied by Giovanardi et al. (2013) and a second one placed in an adjacent area. Particular care has been dedicated to the characterise changes in major and trace element mineral chemistry, as well as in its isotope O, Nd and Sr composition, to document the geochemical fractionation eventually experienced by the flowing melt as a result of the reaction with host peridotite and early cumulates. The genetic and temporal relationships between the dyke emplacement and other events of melt migration recorded by the FPP unit, as well as the related geodynamic scenarios, are also addressed.

Geological setting

In the Finero area (Fig. 1), the IVZ crops out in a pseudo-antiform structure showing the FPP mantle unit at the core, which is flanked by the so-called Finero Mafic Complex (Cawthorn, 1975; Siena & Coltorti, 1989; Lu et al., 1997a, b; Zanetti et al., 2013, 2014; Giovanardi et al., 2014; Mazzucchelli et al., 2014; Langone et al., 2017). The Mafic Complex is divided in three different units: i) the stratigraphically lower Layered Intenal Zone unit (LIZ), in contact with the FPP; ii) the Amphibole-Peridotite (Amph-Pd); and iii) the External Gabbro (EG). The EG is placed in tectonic contact with the Amphibole Peridotite by a Mesozoic high-T shear-zone (Langone et al., 2018). A tectonic contact also characterises the transition towards the amphibolites-facies metasediments and metabasites of the Kinzigite Formation (KF), which represent the metamorphic basement of the Adria plate. Septa of KF rocks are embedded in the EG.

The Finero mafic-ultramafic sequence presents several differences with respect to the southern and central sectors of the IVZ (i.e. the Baldissero and Balmuccia peridotite and the Val Sesia Complex; Quick et at., 1995; Correia et al., 2012; Mazzucchelli et al., 2014 and references therein) providing evidences of a different geological evolution (Zanetti et al., 2013, 2014, 2016; Langone et al., 2017, 2018). In particular, the FPP results completely recrystallized by several events of melt migrations bringing crustal components (Zanetti et al., 1999; 2016; Mazzucchelli et al., 2014 and references therein) and the relationships with the parent melts of the surrounding Mafic Complex are far to be proved (Giovanardi et al., 2014). On the contrary, the peridotites cropping out in the central and southern part of IVZ do not suffered a similar melt-induced recrystallization and were emplaced in the Kinzigite Formation as tectonic slivers before the intrusion of the central and southern Mafic Complex (Quick et at., 1995; Mazzucchelli et al., 2014 and references therein).

The FPP is mainly represented by Phl-bearing Amphibole harzurgites and associated Phl-bearing pyroxenites (Cawthorn, 1975; Siena & Coltorti, 1989; Hartmann & Wedephol, 1993; Zanetti et al., 1999; Raffone et al., 2006; Selverstone & Sharp, 2011; Mazzucchelli et al., 2014; Giovanardi et al.,

129 2018). These lithologies resulted from pervasive metasomatism in a depleted peridotite, which
130 formed secondary Opx, Amph and Phl (Zanetti et al., 1999, Tommasi et al., 2017). Channeled
131 migration events formed dunite bodies containing stratiform to podiform chromitites and, rarely,
132 pyroxenite and hornblendite layers (Grieco et al., 2001, 2004; Zanetti et al., 2016).
133 Late stages of porous-flow melt migrations crystallized Apatite-Dolomite-bearing wehrlites and
134 Apatite-rich orthopyroxene-bearing peridotites, which sometimes contain carbonate-bearing
135 domains showing marked modal and geochemical gradients with the host rocks (Zanetti et al., 1999;
136 Morishita et al., 2003, 2008; Matsumoto et al., 2005; Raffone et al., 2006). U-Pb analyses on Ap
137 and isotopic Noble Gases data provide Triassic ages (Morishita et al., 2008).
138 Apatite and Calcite also occur in dykes of Nepheline-bearing syenites, associated to hornblendites,
139 of Triassic age (Stähle et al, 1990, 2001). Lower Jurassic U-Pb zicon age was determined for an
140 alkali pegmatite (Grieco et al., 2001)
141 The rocks of the FPP related to the main event and the dunite bodies show similar geochemical
142 features and absence of geochemical gradients. The harzburgite-pyroxenite association and the
143 chromitites and pyroxenite layers in dunite bodies are depleted in Nb and HSFE and significantly
144 enriched in K, Rb, Ba, Sr, LREE (Hartmann & Wedephol, 1993; Zanetti et al., 1999, 2016;
145 Mazzucchelli et al., 2014). The mineralogical and compositional features have been considered by
146 several Authors as the evidence of the role of slab-derived crustal component in the percolating
147 melts (Hartmann & Wedephol, 1993; Mazzucchelli et al., 1995; 2016; Rivalenti et al., 1995; 2007a;
148 Zanetti et al., 1999, 2016; Grieco et al., 2001, 2004; Morishita et al., 2003, 2008; Ponce et al., 2015;
149 and others). So far, a variety of different geochemical components has been identified according to
150 the isotopic data. In particular, isotopic Hf (in zircon) and O (in zircon and pyroxenes) composition
151 of chromite minerals points to the presence in the migrating melts of large volumes of continental
152 crust (Zanetti et al., 2016; Malitch et al., 2017), whereas, hydrogen, oxygen and chlorine isotope
153 compositions of Amph and Phl from the harzburgite-pyroxenite association show a variation range
154 (δD from -29 to –86‰, δ^{18}O from 4.9 to 6.1‰ and δ^{37}Cl from -2.0 to +2.1‰) consistent with

mixtures of magmatic fluids with sea-water (Hartmann & Wedepohl, 1993; Selverstone & Sharp, 2011).

Giovanardi et al. (2013) reported the occurrence in the FPP of late Spr-bearing gabbroic dykes. These dykes crosscut at high angle the pervasive mantle foliation and the other lithologies, showing different mineralogical and major element mineral chemistry features with respect to other FPP rocks.

Samples and petrography

Two different dykes and their host peridotites from the FPP unit were investigated. The first dike (sample FI09C06, Fig. 2) was collected along the road that connects the National Road 631 to a peridotite quarry located on the right flank of the Rio Creves valley (less than 100 m far from the outcrops studied by Zanetti et al. 1999), while the second one (FI9664 sample) is from a boulder along the Rio Creves, about 30 m upstream of its intersection with the Rio Cannobino. The host peridotite has been collected 8 cm far from the FI09C06 dyke, and close to the contact with the dyke documented by FI9664 sample.

Gabbroic dykes are centimetric in thickness (mostly 2-5 cm; Fig. 2). They show variable strike, usually crosscutting at high angle the harzburgite-pyroxenite association (Fig. 2).

A Mesozoic age for these Spr-bearing dykes is constrained by the observation they also crosscut the foliation of protomylonites in the external domains of Mesozoic shear zones (Matysiak & Trepmann, 2015 and references therein), but are themselves deformed in a few cm-wide mylonitic to ultramylonitic band parallel to the protomylonites foliation (Tommasi et al., 2017). Such a shear zones were active at different crustal levels over a very long, Triassic-Jurassic time interval (235-180 Ma; Langone et al., 2018 and references therein). This is also consistent with the observation the all the late intrusive bodies discordantly intruding the pervasive mantle foliation by hydraulic fracturing do not show ages older than Triassic (Stähle et al., 1990, 2001; Grieco et al., 2001; Matsumoto et al, 2005).

181 The gabbroic dykes contain Spr (Giovanardi et al., 2013) and show a layered symmetric structure
182 consisting of melanocratic zones at peridotite contacts and a leucocratic zone representing the dyke
183 core (Fig. 2). The melanocratic zones, in turn, can be divided in three different bands.
184 Moving from the host peridotite to the dyke core, the following layers can be recognized:
185 1) an orthopyroxenite zone (hereafter Opx Zone), established within the ambient peridotite. Opx
186 locally shows recrystallized rims with growth of fine neoblasts of Opx and rarely Ol. Opx presents
187 sometimes exsolution lamellae. Locally, black Sp and Phl occur as accessory phase. Phl is
188 concentrated in interstitial position, but rarely, fills fractures within Opx crystals (Fig. 2).
189 Giovanardi et al. (2013) reported the occurrence of Spr-Amph-bearing recrystallisation front also in
190 the Opx Zone.
191 2) a first melanocratic zone (hereafter Early Amph Zone) inside the vein formed by dark-brown
192 Amph (up to 1 cm long, named 'Early Amph') and associated small Plg grains, Sp, Phl and Ap; in
193 these zones the magmatic texture is preserved as evidenced by Amph twinning. Ap and Sp mainly
194 occur as rounded inclusions in Amph, whereas Phl is in interstitial position.
195 3) a second melanocratic zone (hereafter Late Amph Zone), consisting of light-brown to green
196 Amph (named 'Late Amph'), green Sp, Spr and Phl. Spr occurs in three textural positions, namely
197 as: i) inclusions within Late Amph, ii) coronas rimming Sp, and iii) isolated/aggregate crystals in
198 interstitial positions (Fig. 2). Phl is an accessory phase in interstitial positions. Late Amph is smaller
199 than Early Amph, euhedral to anhedral in shape. Intermediate green-brown Amph, often associated
200 with Sp and Spr, is recognized near and through the Early Amph Zone - Late Amph Zone contact.
201 Recrystallization zones with fine-grained texture occur. The Late Amph Zone is not continuous
202 through the dykes. It forms patches, which can occur also only on one side of the leucocratic core of
203 the dyke, or that can extend up to the Opx Zone. The Late Amph Zone is more developed in sample
204 FI9664 (up to about 1.5 cm in thickness) with respect to sample FI09C06 (up to 1 cm in thickness).
205 Besides, Spr crystals in sample FI9664 can reach up to 1.5 mm in size, while in sample FI09C06
206 they are commonly < 0.2 mm.

4) a leucocratic zone (Leucocratic Zone, hereafter) formed by Plg and subordinate Amph (both magmatic and relict from melanocratic zones). Ap occurs as accessory phase, sometimes included in Plg or in relict of brown Early Amph. Rarely Ap contains calcite inclusions. Plg show twinning (mainly Pericline and subordinately crossed Albite-Pericline), which is often partially or totally erased by recrystallisation induced by late deformation. Magmatic Amph has greenish pleochroism whereas relict Amph, ripped from the melanocratic zones, is brown. Amph often forms single-crystal alignments parallel to the dyke strike, like in a flow-texture. Phl is rare and is associated to Amph. Recrystallization zones show fine-grained equigranular texture. Rarely Fe-oxides, Fe-Ni sulphides and pyrite occur.

The host peridotite away from the contact is a hornblende-harzburgite (according to Giovanardi et al., 2018) in modal composition with porphyroclastic texture. It is characterised by the presence of olivine (Ol) and orthopyroxene (Opx) porphyroclasts, with a secondary, undeformed mineral assemblage dominated by amphibole (15% by Vol.), in association with orthopyroxene, spinel, phlogopite and clinopyroxene, strictly similar to the dominant peridotite-type described by Zanetti et al. (1999) and Tommasi et al. (2017). A detailed petrographic inspection highlight the occurrence of a reacted peridotite zone approaching the Opx Zone. It is characterised by the presence of a secondary mineral assemblage, modally dominated by long (up to 5 mm) phlogopite lamellae, to which are associated subordinate amount of undeformed orthopyroxene, spinel, amphibole and clinopyroxene. In the reacted zone, olivine was stable: conversely, the modal orthopyroxene content is slightly lower than in the peridotite far from the vein. Primary (e.g. Olivine) and secondary minerals into the reacted zones display elongation sub-parallel to the present-day vein strike.

Analytical methods

Sample FI9664, representing the gabbroic dyke and the contact host harzburgite, was analyzed for whole rock major and trace elements. Whole rock major elements and Sc, V, Cr, Co, Ni, Cu, Zn

were analysed by X-Ray Fluorescence Spectrometry (XRF), while Li, Rb, Sr, Y, Zr, Nb, Ba, REE, Hf, Ta and Pb were analysed by Inductively Coupled Plasma - Mass Spectrometry (ICP-MS). Analyses were performed following methods described by Mazzucchelli et al. (2010) (data reported in Supplementary material A).

FI9664 and FI09C06 samples were analysed for mineral major element with the electron microprobe JEOL 8200 Super Probe housed at the University of Milano. Analyses were performed following methods described by Ponce et al. (2015). Data are reported in Supplementary Material X.

Mineral trace elements have been determined (as in Rivalenti et al., 2007b) with a LA-ICP-MS housed at I.G.G.-C.N.R., U.O.S of Pavia (data are reported in Supplementary Material Y) using a Perkin Elmer SCIEX DCR-e coupled with a solid-state laser source (Q-switched Nd:YAG, Quantel Brilliant). Data reduction was performed using the GLITTER software. NIST SRM 610 was used as external standard. Ca was used as internal standard for Cpx, Amph and Plg, Si for Ol, Opx and Phl, and Mg for Sp. Precision and accuracy were assessed by repeated analysis of BCR-2g standard, resulting better than 10% relative at ppm concentration level. Further information is reported by Giovanardi et al. (2017).

The sample FI09C06 was selected for determination of O, Nd and Sr isotopic composition in mineral separates, after that the combination of preliminary EMPA and LA-ICP-MS analyses had suggested a more primitive nature for its parent melt.

O isotopes on pure mineral separates from FI09C06 sample were analysed at the I.G.G.-C.N.R., Pisa by conventional laser fluorination with a Finnigan Delta Plus mass spectrometer. 1-1.5 mg aliquots of each phase were necessary to measure the oxygen isotope composition. Analyses were performed following methods described by Perinelli et al. (2011). Data reported in Table 1.

Sr and Nd isotopic ratios on Amph and Plg separates from sample FI09C06 and the host harzburgite were analysed at the laboratories of the Marine Environmental Sciences Laboratory (LEMAR: UBO - CNRS - IRD - Ifremer) of the Institut Universitaire Européen De La Mer (Iuem), Université De

Bretagne Occidentale. Analyses were carried out after dissolution and chromatographic separations using a TRITON Thermo-Ionization Mass Spectrometer (TIMS) following the procedure described in Janin et al. (2012). Analyses were corrected for NBS987 reference material ($^{87}Sr/^{86}Sr$ = 0.710241 ± 0.000019, n = 6) for Sr and La Jolla standard ($^{143}Nd/^{144}Nd$ = 0.511847± 0.000009, n = 3) for Nd. Data reported in Table 2.

Bulk rock chemistry

Gabbroic dyke FI9664 presents higher TiO_2, Al_2O_3, CaO, Na_2O, K_2O, and lower FeO and MgO than the host harzburgite collected at the contact.

The gabbroic dyke has trace element abundances higher than one magnitude order with respect to host harzburgite: only Rb and Li content is similar in both rocks (Fig. 3). The two rock types show some similarities in element fractionation, namely, i) marked enrichments in LREE with respect to M-HREE [$(La/Yb)_N$ is 5.5 and 16-30 for dyke and host harzburgite, respectively; Primitive Mantle data from McDonough and Sun, 1995], ii) $(Th/U)_N$ and $(Zr/Hf)_N$ always <1 and iii) positive Ba and Pb anomaly. Conversely, the $(Nb/Ta)_N$ is 1.6 for the gabbroic dyke and 0.7 for the host harzburgite. gabbroic dyke FI9664.

Linearly-fractionated LREE-enriched patterns are also shown by the nepheline-bearing alkaline dykes described by Stähle et al. (2001). However, these latter possess, in turn, trace element contents significantly higher than that of the gabbroic dyke FI9664. Stahle's dykes also display significant peculiarities in terms of fractionation of highly incompatible trace elements, such as U, Th, Nb, Ta, Ba and Pb, with respect to REE.

The spiderdiagram of the peridotite close to the contact dike FI9664 shows some relevant differences with respect to those reported by Hartmann & Wedephol (1993); i.e. large positive Pb and Hf anomalies, larger Rb, U, Ba, Ta, Nb content, slightly lower LREE content (Fig. 3).

Major element mineral chemistry

285 *Host harzburgites*

286 Mineral composition of the host harzburgite far from the veins is similar to that of the harzburgite-
287 pyroxenite association reported by Zanetti et al. (1999). Amphibole is pargasite in composition,
288 with only one analysis giving Mg-hornblende composition, mica is phlogopite and clinopyroxene is
289 diopside.

290 Minor differences consist in slightly Fe-richer composition shown by Ol [Fo = 100 x Mg / (Mg +
291 Fe^{2+}_{tot}) molar ratio is 90.4-91.1], Opx, Spinel and Amph. Opx and spinel (Hercynite to Spinel in
292 composition) are also richer in Al. Due to their low Cr#, the FI09C06 oxides straddle the Hercynite
293 – Spinel boundary, while oxide in the FPP is Chromite. Lower Cr content is shown by Amph,
294 which is also characterised by lower Na and larger K.

295 At the contact with the vein, the Mg# does not change significantly in the minerals. Aluminium
296 decreases in Opx, Sp, Amph and Phl, while Ti is larger in both Amph and Phl. In Amph, Na
297 decreases, being balanced by larger K. Conversely, the Na/K ratio is very variable in Phl.

298 Opx from the Opx Zone has lower Mg# and CaO and higher Al_2O_3 (Fig. 4). Similarly, its
299 composition is different from the Opx from a Spr-bearing rock found in the LIZ northern unit of the
300 Finero Mafic Complex (Sills et al., 1983): the latter has lower Mg# and higher Al_2O_3 (Fig. 4).

301

302 *Gabbroic dykes*

303 Notwithstanding the similar internal banding, the two studied dykes show marked differences in
304 terms of major element mineral chemistry. Significant compositional changes are also shown for the
305 different types of Amph (i.e. Early, Late and Leuco; Fig. 6). The unique feature of the amphibole
306 major element chemistry common to both gabbroic dykes is the larger Al content exhibited by the
307 Late Amph: this feature was already highlighted by Giovanardi et al. (2013). Amph from gabbroic
308 dykes is mostly Pargasite in compositions (unit formula calculated according to Ridolfi et al.,
309 2018), but sometimes the Al substitution for Si in Late Amph is higher than 2 a.p.f.u., entering in
310 the Sadaganaite compositional field.

311 In particular, Amph from sample FI09C06 has distinctly lower Mg# (0.73-0.82) than in sample
312 FI9664 (0.85-0.87). In sample FI09C06, Mg# is lower in Early Amph than in Late and Leuco
313 Amph, while it is exactly the reverse in sample FI9664 (Fig. 6).
314 FI09C06 Amph also displays the lowest CaO and Na_2O and the highest TiO_2 and K_2O (TiO_2 0.27-
315 2.19 wt.% and 0.31-1.28 wt.% respectively) (Fig. 6).
316 In sample FI09C06, TiO_2 linearly increases with the decrease of Mg#. TiO_2 is instead higher in the
317 FI9664 Early Amph than in the Leuco Amph, but distinctly higher TiO_2 contents are shown by Late
318 Amph. Again in FI9664 Early Amph the increase of Mg# is associated to increasing Cr and Ca, and
319 to decrease of Na and Al.
320 As a whole Amph from gabbroic dykes has higher Al_2O_3 and lower Mg# and Cr_2O_3 with respect to
321 others FPP lithologies, resulting similar to the Amph from the Spr-bearing rock in the LIZ (Sills et
322 al., 1983) (Fig. 6). Amph from the two gabbroic-dykes samples shows lower CaO and K_2O than the
323 respective host Amph and higher Na_2O (Fig. 6).
324 Phl from sample FI9664 presents narrow range of major element contents with respect to sample
325 FI09C06. In sample FI9664, Phl has higher Mg# values with respect to crystals from sample
326 FI09C06 (0.92-0.94 and 0.70-0.90 respectively) and commonly lower TiO_2 (Fig. 5). Phl from the
327 gabbroic dykes shows higher Al_2O_3 and lower Mg# with respect to the Phl from the host peridotite
328 and the harzburgite-pyroxenite association (Fig. 5).
329 Sp is mainly found in the Late Amph Zone. Unlike the Sp from the host harzburgite, the harburgite-
330 pyroxenite association from Zanetti et al. (1999) and the chromitite layers in dunite bodies (Grieco
331 et al., 2001; 2004; Zanetti et al., 2016), the Sp from the gabbroic dykes does not contain Cr_2O_3 and
332 can be classified as Spinel (Mg# 0.46-0.75).
333 Plg from sample FI9664 is commonly more anorthitic with respect to the Plg from sample FI09C06
334 (An content 82-93 and 36-87, respectively). In both samples, some reversely zoned Plg are
335 recognized.

Spr composition falls near the 7:9:3 composition on the SiO_2-(FeO+MgO)-(Al_2O_3+Cr_2O_3+Fe_2O_3) diagram (Fig. 7). Spr from sample FI9664 is higher in Al_2O_3 with respect to sample FI09C06, while is lower in SiO_2.

SEM investigations at the CIGS laboratories of the Università di Modena e Reggio Emilia performed with an ESEM Quanta-200 (Fei Company-Oxford Instruments) suggest that Ap from different zones of the dykes are Cl-apatites.

Trace elements compositions

Host harzburgite

Amph and Cpx from harzburgite FI09C06 8 cm far from the contact are characterised by LREE-enriched linearly fractionated patterns (Fig.s 8, 9 and 10). Their composition is similar to those of the FPP harzburgite-pyroxenite association (Zanetti et al., 1999). Proceeding towards the contact (i.e. FI9664 sample), Amph and Cpx show upward-convex REE patterns characterised by high variability in absolute content (Fig.s 8, 9 and 10). These patterns are similar to those from Ap-rich domains of Zanetti et al. (1999) (Fig.s 9 and 10).

Gabbroic dykes

The two gabbroic dykes show different trace element compositions. In the FI09C06 sample, Amph from the Early Amph Zone and Leucocratic Zone have L-MREE-enriched upward-convex patterns, similar to those of harzburgite near the contact (Fig. 8). In the Late Amph Zone, some crystals show more fractionated pattern characterized by lower M-HREE and positive Eu anomaly (Fig. 8). These variations are associated to a marked depletion in Ta, Zr, Hf, Y and Sc (and V) (Fig. 10). As a whole, Amph from different zones of FI9664 sample show more fractionated REE patterns characterized by enrichment in LREE and depletion in HREE (Fig. 8) with a nearly flat pattern in the LREE region. Amph from Early Amph Zone of sample FI9664 presents a small Eu positive anomaly ($(Eu/Eu^*)_N$ among 1.04-1.65) which become more evident in the Amph from Late Amph

362 Zone ($(Eu/Eu^*)_N$ among 1.29-1.62). Amph from FI9664 sample is also enriched in Th, U and Pb
363 (and in Sr to lesser extent) with respect to FI09C06 ones (Fig. 10).
364 Similarly to Amph, REE patterns of Plg from sample FI9664 are more fractionated than those of
365 Plg from sample FI09C06, (Fig. 8). In both samples, Plg cores are more enriched for absolute
366 element abundances than Plg rims.
367 Ap displays the typical LREE enrichment and large Th, U and Pb contents (12.31-17.35 ppm, 4.35-
368 5.92 ppm and 2.18-4.19 ppm, respectively). Nb, Ta, Zr, Hf, Ti and Sc form negative anomalies
369 whose values are often below detection limit.
370 No systematic trace elements variations are found in Phl.
371
372 **O isotopes**
373 The $\delta^{18}O$ in FI09C06 silicates shows a steady increase from the contact (Opx-zone) to the
374 Leucocratic gabbro in the vein core, through the Early and Late Amph Zones (Fig. 11). In
375 particular, it varies from 5.81‰, std. dev. 0.11, in Opx from Opx Zone, to 6.9‰, std. dev. 0.05, in
376 Amph from the Early and Late Amph Zones, to 8.60‰, std. dev. 0.01, in the Plag of the gabbroic
377 core.
378 The $\delta^{18}O$ of Opx from Opx Zone lies within the mantle range. They are higher than the $\delta^{18}O$ value
379 reported by Hartmann & Wedephol (1993) for Cpx from the Phl-bearing Amphibole harzburgite
380 (Fig. 11), and for Opx from Ol-chromitites of FPP, but significantly lower than the Opx-from Opx-
381 chromitites (Zanetti et al., 2016).
382 Vein Amph and Plg have $\delta^{18}O$ values significantly higher than mantle range (Fig. 11). They are
383 close to the highest found in Amph, Phl, Opx, Cpx and Zrc from the Phl-bearing Amphibole
384 harzburgites-pyroxenites (Hartmann & Wedephol, 1993; Selverstone and Sharp, 2011) and
385 chromitite layers of FPP (Zanetti et al., 2016).

386 The $\delta^{18}O$ obtained for the green spinel associated to sapphirine is markedly lower than those of
387 associated Late Amph ($\delta^{18}O$ = 4.38‰, std. dev. 0.10), as expected due to crystal-chemical
388 constraints (see Bindeman, 2008 and references therein).
389
390 **Sr and Nd isotopes**
391 The trace element concentrations of the mineral separates of Early and Late Amph matches the
392 differences highlighted by LA-ICP-MS on thin section. The Sr and Nd isotopic compositions of
393 Early Amph and Late Amph from FI09C06 dyke are coincident within the analytical uncertainty
394 (Table 2). Plagioclase from the FI09C06 Leuco Zone shows the same Sr isotopic composition of the
395 amphiboles, and only slightly more radiogenic. Similar Sr isotopic compositions were documented
396 in Amph and Ap from discordant veins from FPP, which are characterised by higher Nd^{143}/Nd^{144}
397 (Morishita et al., 2008). The isotopic composition of dyke minerals is enriched with respect to
398 Depleted Mantle and MORB values, falling in the OIB field (Fig. 12). In particular, they lie
399 between the isotopic compositions of FPP hornblende-syenite dykes (bulk rock from Stähle et al.,
400 1990, 2001) and peridotites (Amph and Cpx from Obermiller, 1994). Amph separated from the host
401 harzburgite (collected far from the contact) show the most enriched radiogenic Sr and unradiogenic
402 Nd values never documented in literature for FPP rocks, considering both peridotites and dykes
403 (Fig. 12).
404
405 **Discussion**
406
407 **1) Constraints on Melt Percolation through Peridotite**
408 The two veins here studied share exactly the same internal banding of the sample described by
409 Giovanardi et al. (2013). This suggests that all the three veins were part of an interconnected
410 swarm, and this allowed to record the same sequence of petrologic events. According to the process
411 governing the emplacement of other dyke swarms in mantle sectors (e.g. Mazzucchelli et al., 2010

412 and references therein), it is considered that the melt flowing in the metasomatic haloes and in the
413 conduit was originally similar, suffering severe fractionation due to Assimilation and Fractional
414 Crystallisation. Exceptions will be highlighted and discussed.
415 The characterisation of the wall peridotite has revealed some peculiarities. It is a common
416 observation that metasomatic haloes of cm-to-m-scale wrapped out late dykes and veins formed by
417 melt segregation at mantle conditions. In most cases, the metasomatic haloes show marked
418 geochemical and mineralogical gradients as a function of the distance from the dike contact (Zanetti
419 et al., 1996; Ionov et al., 2002, Mazzucchelli et al., 2010; Borghini et al., 2016, 2017), which are
420 interpreted as the result of porous flow percolation of melt escaping from the open conduits.
421 Conversely, no progressive mineralogical or compositional variation is documented into the wall
422 peridotite FI9664 at variable distance from the vein (see Supplementary material B). Newly-formed
423 clinopyroxene actually shows trace element heterogeneities, but these are randomly distributed.
424 Conversely, trace element composition of Amph is very homogeneous, indicating a late
425 crystallisation from a unique melt.
426 The peculiar L/MREE-enriched convex-upward patterns shown by Cpx and Amph from the wall
427 peridotite FI9664 also evidence that their parent melt could not be the same from which crystallised
428 the adjacent Early Amph in dyke FI9664 (which show linearly-fractionated REE patterns).
429 However, according to Amph trace element composition, the melt recorded by the wall peridotite
430 FI9664 had to be quite similar to that producing the Early Amph Zone of dyke FI09C06.
431 The textural evidence that primary and secondary minerals into the metasomatic haloes display
432 elongation sub-parallel to the present-day vein strike confirms that the development of melt
433 migration channels was associated to some local deformation.
434 These observations can be reconciled assuming that the metasomatic haloes were not produced by
435 melt escaping normally from the conduit. They were likely established during an early stage of melt
436 migration occurred via focused porous flow along channels developed in correspondence of
437 structural weakness, whose direction was roughly parallel to the strike of the present-day veins.

438 Detailed petrographic inspection indicates that in the reacted wall peridotite olivine was stable.
439 Conversely, the modal content of orthopyroxene is slightly lower than in the peridotite far from the
440 vein. This evidence brings us to consider that the Opx-saturation of the melts indicated by the
441 segregation of reactive Opx Zone and the presence of few Opx in the veins (Giovanardi et al., 2013)
442 was not a clear, primary characteristic, but possibly a consequence of early stage of reactive melt
443 migration characterised by olivine–precipitation and orthopyroxene dissolution (see Piccardo et al.,
444 2017).
445 Besides, the mineralogical mismatch between the nearly monomineralic, hydrous-mineral-free Opx
446 Zone and the Early Amph Zone suggests that they were segregated by the melts compositionally
447 different. This hypothesis is confirmed by large differences in terms of isotope O composition
448 recorded by Opx (5.8‰ SMOW) from Opx Zone and the Early Amph Zone (6.9‰ SMOW) within
449 the vein. The lighter isotope O composition of the Opx Zone would support a hybrid composition of
450 its parent melt due to reactive porous flow through the FPP, with buffering of isotope O
451 composition at mantle values.
452 This conclusion brings us to take into consideration the possibility that Opx-Zone formed before the
453 segregation of the Amph Zones, possibly ad the centre of the migration channels, as observed
454 elsewhere in the FPP. It was successively split in two parts by the opening of the fracture.
455
456 **2) Melt segregation in the open conduit**
457 Early Amph was segregated when melts started flowing in actually open fractures. It is likely that
458 Amph crystallisation was triggered by the presence of an ultramafic wall, suggesting that Plg was
459 unstable in contact with the orthopyroxenite layers. The development of Amph-rich selvages has
460 been already documented in literature, where hydrous gabbroic rocks come in contact with
461 ultramafic layers (e.g. in the LIZ of Finero Complex, Mazzucchelli et al., 2014). Moreover, it is a
462 common observation that in dykes/veins produced by percolation of late hydrous melts/fluids
463 through oceanic gabbroic rocks, Amph grows in correspondence of wall Cpx, whereas new Plg

segregates in textural positions in which the wall mineral is previous Plg (Cortesogno et al., 2004; Tribuzio et al., 2014).

The vein minerals of this study show significant differences in terms of major and trace element mineral compositions. In particular, Amph from FI9664 vein shows a peculiar relative enrichment in highly incompatible trace elements (U, Th, LREE, Na) and compatible elements (Mg, Ca and Cr) with respect to those from FI09C06 vein. Consistently, Phl is Mg-Na-richer and Plg is more anorthitic. Assuming that the dyke swarm was produced by the injection of the unique melt, this relationship cannot be reconciled by a melt evolution only governed by fractional crystallisation. Mazzucchelli et al. (2010) documented the same correlation between compatible and incompatible elements in minerals from cm-thick diorite dykes demonstrating that such geochemical features can be modelled considering an assimilation of host minerals concomitant to fractional crystallisation. Accordingly, we argue that the parent melt of vein minerals FI9664 can be considered more evolved than that of dyke FI09C06 through AFC process. The concomitant enrichment of Na and Ca in the FI9664 vein minerals evidence the role of Amph in the assimilated component. This is also confirmed by the trace element patterns of FI9664 vein amphiboles, in which highly incompatible elements, such as LREE, Th and U, increase, whereas moderately incompatible element such as HREE, Ti and Y decrease, moving towards the fractionation shown by those of host harzburgite away from the contact. The decrease of moderately incompatible elements with the progression of the melt evolution may be indicative of $^{Amph/L}D$ higher than 1 (Tiepolo et al., 2007). It is noteworthy that the Al content in FI9664 Early Amph is comparable to slightly lower than in those from FI09C06 vein, suggesting that the assimilation of host minerals was not effective in boosting the Al concentration the evolving melt.

a) Formation of Sapphirine-bearing patches

The petrographic features of the Sapphirine-bearing zones documented on samples are similar to those described by Giovanardi et al. (2013).

490 The mm-to-cm-thick Sapphirine-bearing patches and stripes are randomly distributed from the
491 internal end of the hornblendite seam to the Opx Zone, even tough are basically concentrated
492 towards the centre of the veins. They are apparently the results of interstitial migration of a melt
493 chemically in disequilibrium with the early cumulus minerals, as testified by actual recrystallization
494 fronts inside large Early Amph. Both interstitial and recrystallized patches show that the injected
495 melt was saturated in Late Amph, Spr and Sp, whereas the saturation in Phl is uncertain, because it
496 occurs only interstitially, and the textural relationships are not unequivocal.
497 The following series of petrographic and geochemical features suggest that the sapphirine-bearing
498 mineral assemblages were not simply related to interaction with the parent melt of the Leucocratic
499 Zone, but segregated because of the injection in the dykes swarm of an additional melt component
500 coming from outside of the system:

501 1) Early Amph at the contact with or embedded by the plagioclase of the Leuco Zone does not
502 show any evidence of comparable reaction;
503 2) Notwithstanding the significantly different major element composition of Early Amph
504 documented in the two veins of this study, the major element chemistry of Spr-associated
505 Late Amph converge towards specific Al and Mg# values. Phlogopite shows a consistent
506 variation, even though its attribution to Early or Late Amph assemblages is doubtful because
507 of its interstitial position. The data reported by Giovanardi et al. (2013) confirm the trend.
508 This indicates that a unique component with a specific composition was responsible of the
509 Spr segregation in the three sectors of the dyke swarm.
510 3) Normalised patterns of Late Amph from Spr-bearing areas shows peculiar features, namely
511 stronger LREE/HREE fractionation, depletion in M-HREE, Zr, Hf, Nb, Ta,Ti, Sc and V, and
512 the appearance of positive Eu anomaly. It is also observed the inversion of the $(Zr/Hf)_N$,
513 which is >1 in the Early Amph, but <1 in the Late Amph. The overall fractionation mimics
514 that normally exhibited by Plg.

515 This evidence, consistently with the apparent increase of the Al content in the system, suggests
516 that the injected melt contained large volumes of Plg component.
517 Isotopic O, Nd and Sr compositions of Early and Late Amph are very similar, suggesting that
518 the Plg component belonged to the same magmatic cycle producing the dyke swarm.
519 On the other hand, petrographic survey has never provided evidence of Plg assimilation and/or
520 replacement by Amph or whatever, excluding that the Plg component derived by local
521 assimilation. Thus, it is envisaged that the Plg signature was acquired by the injected melt
522 through: 1) assimilation of cumulus Plg in hidden magmatic bodies; 2) addition in the melt
523 source, where it was likely present has high-P metamorphic equivalent of pristine Plg.
524
525 **b) The Leucocratic Zone**
526 The petrographic evidence confirms that the formation of the Leucocratic layers was a high energy
527 event, which determined the partial disaggregation of the Early Amph layers, with evident breaking
528 of large Early Amph crystals. It can be locally recognised that two parts of a formerly unique crystal
529 apparently lie on different sides of a vein. Giovanardi et al. (2013) suggested that this stage was
530 accompanied by enlargement of the conduits.
531 The Nd and Sr isotopic composition of Plg indicates that the parent melt had a cognate origin with
532 those of the hornblendite selvages. This is also confirmed by the trace element composition of the
533 Leucocratic Amph, which is strictly similar to that of the associated Early Amph.
534 Nevertheless, the observation that the major element chemistry of Leucocratic Amph is
535 intermediate between that of Early and Late Amph, brings has to conclude that the parent melt of
536 the Spr-bearing assemblages could be still present in diluted proportions.
537
538 **3) Nature of the parent melts**
539 The assessment of the nature of the parent melt of magmatic segregates belonging to narrow, cm-
540 thick veins/dykes intruding mantle peridotites at high-T-P mantle conditions must be done with

541 particular caution, trying firstly to characterize the modifications imparted by fractional
542 crystallization of minerals and the reaction/assimilation with the host rock (e.g. Mazzucchelli et al.,
543 2010 and references therein).

544 **a) Isotope O composition**

545 An important contribution about the definition of the geochemical components in the upcoming
546 melts is provided by the marked zoning in terms of isotopic O composition documented in the
547 sample FI09C06 among i) the Opx Zone, ii) the hornblendite selvage and iii) the Leucocratic Zone.
548 The $\delta^{18}O$ values of Early and Late Amph (6.9 ‰ SMOW) are well-exceeding the mantle range
549 (Bindeman, 2008; Polat et al., 2018), pointing to large volumes of crustal component in the parent
550 melt of FI09C06 hornblendite. The proportion of crustal component still increases into the
551 leucocratic layer, where a $\delta^{18}O$ value of 7.8 ‰ SMOW can be calculated for the Amph in
552 hypothetical equilibrium with the Plg composition (8.6‰ SMOW), conservatively considering i) a
553 low closure T for FPP of ~850°C (provided by pyroxene-solvus geothermometers), ii) an average
554 value of An70 for plagioclase and iii) the $\delta^{18}O$ mineral fractionation values reported by Bindeman
555 (2008).
556 Literature data on FFP minerals show a pronounced heterogeneity in merit to the isotopic O
557 composition, with $\delta^{18}O$ values from below to well-above the mantle range (Hartmann and
558 Wedephol, 1993; Selverstone and Sharp, 2011; Zanetti et al., 2016). This is an apparent result of
559 multiple melt-migration events.
560 Values of $\delta^{18}O$ approaching that Early and Late Amph have been sometimes documented in
561 harzurgites and chromitites (Hartmann & Wedephol, 1993; Zanetti et al., 2016), but the values of
562 the Leucocratic layers are markedly out of range.
563 Besides, the $\delta^{18}O$ value shown by Opx (5.81 ‰ SMOW) from the Opx Zone provides a very
564 important constraint, indicating as migrating melts, after prolonged interaction with FPP, may have
565 isotopic oxygen composition buffered to the mantle range. The decrease of $\delta^{18}O$ values in the

minerals from the hornblendite selvages with respect to those from dyke core, i.e. the Leucocratic Zone, confirms such a buffering effect.

It is concluded that the high $\delta^{18}O$ shown by dyke minerals cannot apparently be the result of interaction between melts and FPP. It was a primary feature of the melts, indicating the occurrence of large amounts of crustal components, which must have been added to the melt in the source regions or, anyway, at deeper mantle depths.

Subduction-related component was identified on the basis of Noble Gases isotopic composition in late, Triassic apatite-rich layers (Matsumoto et al., 2005, Morishita et al., 2003, 2008), overprinting the crustal affinity of the host FPP. Amphiboles from such Ap-layers show the same radiogenic Sr composition of FI09C06 minerals, coupled to slighter more radiogenic Nd composition.

The isotopic composition of Early Amph, Late Amph and Plag from FI09C06 dyke is significantly richer in radiogenic Sr and unradiogenic Nd with respect to those reported by nepheline-bearing Triassic intrusions cutting the FPP (Stähle et al., 1990, 2001), which were interpreted as derived by alkaline melts of OIB-affinity.

The combination of the data of nepheline-bearing alkaline dykes, the Spr-bearing dykes and FFP data define a trend at low radiogenic Nd and large radiogenic Sr, suggesting a mixing between asthenospheric components (OIB, according to Stähle et al., 1990; 2001 and Schaltegger et al., 2015) with components derived from continental crust (see compositional fields in Casetta et al. 2018a). It is apparent that such a trend is approached by the Sr and Nd isotopic composition of Triassic K-rich calc-alkaline to shoshonitic intrusive rocks and lavas of the Eastern Alps (Casetta et al., 2018a; Figure 12).

Speculatively, it can be considered that the crustal components were seated at lithospheric deep levels after the Variscan orogenic cycle (e.g. Bonadiman et al., 1994) and mobilized by asthenospheric magmatism. This scenario is supported by the evidence of continental crustal metasomatism exhibited by mantle bodies involved in the Variscan collisional orogeny, such as

591 FPP, Ulten (Sapienza et al., 2009) and some of the Bohemian Massif (Becker et al., 1999;
592 Schulmann et al., 2014).
593 In this frame, it can be noted that the FI09C06 isotopic compositions of Sr and Nd lie on the mixing
594 line between the composition of the Triassic alkaline dykes and the host harzburgite far from the
595 contact. According to AFC simulation, assimilation of significant degrees of the metasomatised
596 peridotite material (15%) into OIB must be taken into account to document the composition of the
597 parent melt of FI09C06 veins.

598 **c) Trace elements**

599 The comparison of the trace element patterns of the Amph from the vein apparently less
600 contaminated by the host peridotite (FI09C06) with those of amphiboles segregated by primary
601 hydrous alkaline basalts (e.g. Demeny et al., 2005) evidences similarity in REE fractionation, but
602 the Early Amph have absolute content nearly one magnitude order higher. Besides, a correlation
603 with primary alkaline mantle melts is not straightforwardly supported by the negative Nb-Ta-Ti
604 anomalies shown by Early Amph.
605 Equilibrium liquids calculated on the basis the trace element composition of Early Amph from
606 Fi09C06 dyke and amphibole-melt partition coefficients experimentally determined for T of
607 1015°C in presence of moderately polymerized melts (dataset T2 1015; Tiepolo et al., 2007), match
608 the REE content and fractionation exhibited by Shoshinitic rocks of the Triassic magmatism of the
609 Dolomitic areas (Casetta et al., 2018a; 2018b; see Supplementary material C). The calculated melts
610 also show consistent negative Ti anomalies and $(Nb/La)_N$ close to 1, and slight positive U, Th and
611 Pb anomalies: the latter are more pronounced in the shoshonitic melts. However, a best match in
612 terms of U, Th and Pb concentrations is shown by equilibrium liquids calculated in equilibrium
613 with amphiboles from the 9664 dykes. These observations suggests that the Spr-bearing gabbroic
614 dykes may be the record of the deep mantle input to the Triassic K-rich calc-alkaline to shoshonitic
615 melts erupted into the Eastern Southern Alps, also documenting the fractionation trends responsible
616 for the enrichment in Th, U and Pb.

617

618 **4 Constraints on the Geodynamic evolution of the Europe-Africa boundary**

619 a) P-T constraints on FPP

620 Geothermobarometric estimates constrain the intrusion of Spr-bearing dykes at very high-P and T
621 conditions. Ab-initio calculations indicate that primary crystallization field of Spr in the MAS
622 diagram (SiO_2-MgO-Al_2O_3) becomes definitely larger over 1.0 GPa, shrinking at 2.0 GPa
623 (Belmonte et al., 2014). This evidence confirms the experimental results of Liu & Presnall (1990,
624 2000) and Milholland & Presnall (1998), indicating that magmatic Spr in FPP veins likely
625 crystallised at $P \geq 1$ GPa. Equilibrium T estimated with the Spr-Sp Mg-Fe^{2+} exchange thermometer
626 of Sato et al. (2006) and with the Amph-Plg thermometer of Holland & Blundy (1994) are mostly
627 higher than 1000°C (up to 1085°C), confirming the T estimates of Giovanardi et al. (2013). The
628 melt T was thus significantly higher than host harzburgite, which shows solidus T typically
629 corresponding to that of the water-oversaturated peridotite (965°C at P = 1.1 GPa; Giovanardi et al.,
630 2013). The absence of evidence for partial melting in the host FPP confirms that the source of the
631 uprising melts was at greater, mantle depths. The high T, in combination with the large water and
632 volatile contents, may have allowed the melt to migrate via porous-flow along direction of
633 structural weakness (see Tommasi et al., 2017), before the opening of the conduits.
634 The high-P emplacement conditions are consistent with the scenario for which after Paleozoic
635 metasomatism the FPP remained at greater depths than the large lherzolitic mantle bodies South of
636 the Anzola-Val Grande High-T shear zone (namely, from North to South, Premosello, Balmuccia
637 and Baldissero; Quick et al., 1995), until its exhumation at shallower levels at ~180 Ma (Zanetti et
638 al., 2013, 2016; Langone et al., 2017, 2018; Decarlis et al., 2017, Malitch et al., 2017; Petri et al.,
639 2019).

640

641 **b) Constraints on the Mesozoic mantle sources at the Africa-Europe Boundary**

642 The outcomes of this study indicate that in Mesozoic times, melts extremely rich in volatiles (H_2O,
643 P, CO_2 and Cl), K, Na and highly-incompatible element rose up from the mantle depths towards the
644 surface. The large amount of the crustal components present in the melts, as testified by the O
645 isotopic composition, bring us to consider that their large Al content, the enrichment in LILE and
646 LREE, and the enriched Nd and Sr isotopic composition consistent were basically a primary feature
647 inherited from the source.
648 This finding confirms the extreme complexity of the tectono-magmatic scenario recorded by the
649 FPP. In particular, it evidences as the Northern IVZ records an extremely prolonged release (lasted
650 from the Variscan orogenic cycle to the Mesozoic exhumation of lithospheric mantle at shallower
651 levels) of K-H_2O-rich mantle-derived melts polluted by subduction-related components. This
652 explains why FPP records many generations of Phl-bearing mineral assemblages, showing variable
653 filed relationships, geochemical signature and ages (Hartmann & Wedeohol, 1993; Zanetti et al.,
654 1999; 2013; 2016; Stähle et al., 1990; 2001; Greco et al., 2001;2004; Morishita et al., 2003, 2008;
655 Malitch et al., 2017). It also provides a new interpretative frame to previous data indicating the
656 emplacement of melts with subduction-related components in Triassic times (Mastumoto et al.,
657 2005; Morishita et al., 2008, Malitch et al., 2017)
658 Such a magmatism bearing subduction component appears roughly overlapped to the ascent of
659 silica-undersaturated alkaline melts of OIB-affinity (Stähle et al., 1990, 2001, Schaltegger et al.,
660 2015), which likely have some counterparts also in the Central IVZ (Fiorentini et al., 2018; Galli et
661 al., 2019).
662 It developed in a concomitant extensional-transtensional tectonic regime, whose origin and
663 geodynamic scenario are still strongly debated (Cassinis et al., 2008; Zanetti et al., 2013; Casetta et
664 al., 2018a,b)
665 Further investigations are needed to address the issues whether crustal components are remnants of
666 old subduction events (Bonadiman et al., 1994), possibly located at lithospheric levels, reactivated
667 by asthenospheric magmatism with OIB or DM affinity, or whether they were crustal material

668 recycled into asthenospheric mantle sources (Locmelis et al., 2016), or related to the addition of
669 crustal components in relation to some active Mesozoic subduction (Cassini et al., 2008; Schmid et
670 al., 2008; Morishita et al., 2008; Selverstone and Sharp, 2011; Zanetti et al., 2013).
671 It is a matter the fact that the major (in particular the enriched composition in K and Al), trace and
672 Sr and Nd isotopic composition of the sapphirine-bearing gabbroic rocks approach the geochemical
673 feature shown by Triassic K-rich calc-alkaline to shoshonitic magmatism of the Dolomites area
674 (eastern Alps) (Casetta et al., 2018a,b). Thus, it is confirmed that the study of the magmatic events
675 at the roots of the continental crust of the Adria plate can provide a unique opportunity to constrain
676 the tectono-magmatic evolution of at the Europe-Africa boundary.
677

678 **Concluding remarks**

679 New, very detailed surveys on Mesozoic Spr-bearing gabbroic dykes within the FPP unit led to
680 describe different stages of melt migration (from porous-flow migration in peridotite channels to
681 flow in open conduits) and constrain the presence in the parent melts of large amounts of
682 continental crustal components that were acquired in the source region or at deeper lithospheric
683 mantle levels.
684 The reaction between dyke melts and the strongly metasomatised FPP enhanced the crustal
685 signature.
686 The large Al content of these melts allowed for the segregation of magmatic sapphirine, which is
687 marker of high-P-T conditions of intrusion.
688 This dyke swarm possibly represents a record of the mantle input to the K-rich calk-alkaline to
689 shosonitic magmatism widespread during Triassic in the Southern Alps area.
690

691 **Acknowledgements**

692 This work was supported by MIUR PRIN 2015 Prot. 20158A9CBM.
693

694 **References**

695 Becker, H., Wenzel, T., Volker, F. (1999). Geochemistry of glimmerite veins in peridotites from
696 Lower Austria - implications for the origin of K-rich magmas in collision zones. Journal of
697 Petrology, 40, 315-338.

698 Belmonte, D., Ottonello, G., Zuccolini, M.V. (2014). Ab initio thermodynamic and thermophysical
699 properties of sapphirine end-members in the join $Mg_4Al_8Si_2O_{20}$-$Mg_3Al_{10}SiO_{20}$. American
700 Mineralogist, 99, 1449-1461.

701 Bindeman, I. (2008). Oxygen Isotopes in Mantle and Crustal Magmas as Revealed by Single
702 Crystal Analysis. Reviews in Mineralogy & Geochemistry, 69, 445-478.

703 Bonadiman, C., Coltorti, M., Siena, F. (1994). Petrogenesis and T-fO_2 estimates of Mt. Monzoni
704 complex (Central Dolomites,Southern Alps): a Triassic shoshonitic intrusion in a transcurrent
705 geodynamic setting. European Journal of Mineralogy, 6, 943-966.

706 Borghini, G., Rampone, E., Zanetti, A., Class, C., Cipriani, A., Hofmann, A.W., Goldstein, S.L.
707 (2016). Pyroxenite layers in the Northern Apennines' upper mantle (Italy) - generation by
708 pyroxenite melting and melt infiltration. Journal of Petrology, 57, 625-653

709 Borghini, G., Fumagalli, P., Rampone E. (2017). Partial melting of secondary pyroxenite at 1 and
710 1.5 GPa, and its role in upwelling heterogeneous mantle. Contributions to Mineralogy and
711 Petrology, 172, 70, https://doi.org/10.1007/s00410-017-1387-4.

712 Casetta, F., Coltorti, M., Ickert, R.B., Bonadiman, C., Giacomoni, P.P., Ntaflos, T. (2018a).
713 Intrusion of shoshonitic magmas at shallow crustal depth: T–P path, H_2O estimates, and AFC
714 modeling of the Middle Triassic Predazzo Intrusive Complex (Southern Alps, Italy). Contributions
715 to Mineralogy and Petrology, 173, 57, https://doi.org/10.1007/s00410-018-1483-0.

716 Casetta, F., Coltorti, M., Marrocchino, E. (2018b). Petrological evolution of the Middle Triassic
717 Predazzo Intrusive Complex, Italian Alps. International Geology Review, 60, 977-997.

718 Cassinis, G., Cortesogno, L., Gaggero, L., Perotti, C. R., Buzzi, L. (2008). Permian to Triassic and
719 magmatic evolution of theBrescian Prealps (eastern Lombardy, Italy). Italian Journal of
720 Geosciences, 3, 501-518.
721 Cawthorn, R.G. (1975). The amphibole peridotite - metagabbro complex, Finero, northern Italy.
722 Journal of Geology, 83, 437-454.
723 Correia, C.T., Sinigoi, S., Girardi, V.A.V., Mazzucchelli, M., Tassinari, C.C.G., Giovanardi, T.
724 (2012). The growth of large mafic intrusions: Comparing Niquelândia and Ivrea igneous complexes.
725 Lithos, 155, 167-182.
726 Cortesogno, L., Gaggero,L., Oggiano, G., Paquette, J.-L., (2004). Different tectono-thermal
727 evolutionary paths in eclogitic rocks from the axial zone of the Variscan chain in Sardinia (Italy)
728 compared with the Ligurian Alps. Ofioliti, 29, 125-144.
729 Decarlis, A., Beltrando, M., Manatschal, G., Ferrando, S., Carosi, R. (2017). Architecture of the
730 distal Piedmont-Ligurian rifted margin in NW Italy: Hints for a flip of the rift system polarity.
731 Tectonics, 36, 2388-2406.
732 Demény, A., Vennemann, T.W., Homonnay, Z., Milton, A., Embey-Isztin, A., Nagy, G. (2005).
733 Origin of amphibole megacrysts in the Pliocene-Pleistocenebasalts of the Carpathian-Pannonian
734 region. Geologica Carpathica, 56, 179-189.
735 Dohmen, R., Blundy, J. (2014). A predictive thermodynamic model for element partitioning
736 between plagioclase and melt as a function of pressure, temperature and composition. American
737 Journal of Science, 314, 1319–1372.
738 Fiorentini, M.L., LaFlamme, C., Denyszyn, S., Mole, D., Maas, R., Locmelis, M., Caruso, S., Bui,
739 T.-H. (2018). Post-collisional alkaline magmatism as gateway for metal and sulfur enrichment of
740 the continental lower crust. Geochimica et Cosmochimica Acta, 223, 175-197.
741 Galli, A., Grassi, D., Sartori, G., Gianola, O., Burg, J.-P., Schmidt, M.W. (2019). Jurassic
742 carbonatite and alkaline magmatism in the Ivrea zone (European Alps) related to the breakup of
743 Pangea. Geology, 47, 1–4, https://doi.org/10.1130/G45678.1.

744 Giovanardi, T., Morishita, T., Zanetti, A., Mazzucchelli, M., Vannucci, R. (2013). Igneous
745 sapphirine as a product of melt-peridotite interactions in the Finero Phlogopite-Peridotite Massif,
746 Western Italian Alps. European Journal of Mineralogy, 25, 17-31.
747 Giovanardi, T., Mazzucchelli, M., Zanetti, A., Langone, A., Tiepolo, M., Cipriani, A. (2014).
748 Occurrence of Phlogopite in the Finero Mafic Layered Complex. Central European Journal of
749 Geosciences, 6(4), 588-613.
750 Giovanardi, T., Girardi, V.A.V., Correia, C.T., Sinigoi, S., Tassinari, C.C.G., Mazzucchelli, M.
751 (2017). The growth and contamination mechanism of the Cana Brava layered mafic-ultramafic
752 complex: new field and geochemical evidences. Mineralogy and petrology, 111, 291-314.
753 Giovanardi, T., Freddo, I., Mazzucchelli, M. (2018). Filling the Gap in the Classification of
754 Phlogopite-Bearing Ultramafic Rocks. The Journal of Geology, 126, 361–370.
755 Grieco, G., Ferrario, A., von Quadt, A., Köppel, V., Mathez, A. (2001). The zircon-bearing
756 chromitites of the phlogopite peridotite of Finero (Ivrea Zone, Southern Alps): evidence and
757 geochronology of a metasomatized mantle slab. Journal of Petrology, 42/1, 89-101.
758 Grieco, G., Ferrario, A., Mathez, E.A. (2004). The effect of metasomatism on the Cr-PGE
759 mineralization in the Finero Complex, Ivrea Zone, Southern Alps. Ore Geology Reviews, 24, 299-
760 314.
761 Hartmann, G. & Wedepohl, K.H. (1993). The composition of peridotite tectonites from the Ivrea
762 Complex, northern Italy: Residues from melt extraction. Geochimica et Cosmochimica Acta, 57,
763 1761-1782.
764 Higgins, J.B., Ribbe, R.H., Herd, R.K. (1979). Sapphirine I. Crystal chemical contributions.
765 Contribution to Mineralogy and Petrology, 68, 349-356.
766 Holland, T. & Blundy, J. (1994). Non-ideal interactions in calcic amphiboles and their bearing on
767 amphibole-plagioclase thermometry. Contributions to Mineralogy and Petrology, 116, 433-447.

768 Ionov, D.A., Bodinier, J.-L., Mukasa, S.B., Zanetti, A. (2002). Mechanisms and sources of mantle
769 metasomatism: major and trace element compositions of peridotite xenoliths from Spitsbergen in
770 the context of numerical modelling. Journal of Petrology, 43, 1-41.
771 Janin, M., Hémond, C., Maia, M., Nonnotte, P., Ponzevera, E., Johnson, K.T.M. (2012). The
772 Amsterdam–St. Paul Plateau: A complex hot spot/DUPAL-flavored MORB interaction.
773 Geochemistry Geophysics Geosystems, 13-9, 10.1029/2012GC004165.
774 Langone, A., Padrón-Navarta, J. A., Ji, W.-Q., Zanetti, A., Mazzucchelli, M., Tiepolo, M.,
775 Giovanardi, T., Bonazzi, M. (2017). Ductile-brittle deformation effects on crystal-chemistry and U-
776 Pb ages of magmatic and metasomatic zircons from a dyke of the Finero Mafic Complex (Ivrea-
777 Verbano Zone, Italian Alps). Lithos, 284-285, 493-511.
778 Langone, A., Zanetti, A., Daczko, N.R., Piazolo, S., Tiepolo, M., Mazzucchelli, M. (2018). Zircon
779 U-Pb dating of a lower crustal shear zone: A case study from the northern sector of the Ivrea-
780 Verbano Zone (Val Cannobina, Italy). Tectonics, 37, 322–342.
781 Liu, T.C. & Presnall, D.C. (1990). Liquidus phase relationships on the join anorthite-forsterite-
782 quartz at 20 kbar with applications to basalt petrogenesis and igneous sapphirine. Contributions to
783 Mineralogy and Petrology, 104, 735-742.
784 Liu, T.C. & Presnall, D.C. (2000). Liquidus phase relations in the system CaO-MgO-Al2O3-SiO2
785 at 2.0 GPa: applications to basalt fractionation, eclogites, and igneous sapphirine. Journal of
786 Petrology, 41, 3-20.
787 Locmelis, M., Fiorentini, M.L., Rushmer, T., Arevalo Jr, R., Adam, J., Denyszyn, S.W. (2016).
788 Sulfur and metal fertilization of the lower continental crust. Lithos, 244, 74-93.
789 Lu, M., Hofmann, A.W., Mazzucchelli, M., Rivalenti, G. (1997a). The mafic-ultramafic complex
790 near Finero (Ivrea-Verbano zone), I. Chemistry of MORB-like magmas. Chemical Geology, 140,
791 207-222.

792 Lu, M., Hofmann, A.W., Mazzucchelli, M., Rivalenti, G. (1997b). The mafic-ultramafic complex
793 near Finero (Ivrea-Verbano zone), II. Geochronology and isotope geochemistry. Chemical Geology,
794 140, 223-235.
795 Lyubetskaya, T., Korenaga, J. (2007). Chemical composition of Earth's primitive mantle and its
796 variance: 1. Method and results. Journal of Geophysical Research 112, B03211.
797 Malitch, K.N., Belousova, E.A., Griffin, W.L., Badanina, I.Yu., Knauf, V.V., O'Reilly, S.Y.,
798 Pearson, N.J., 2017, Laurite and zircon from the Finero chromitites (Italy): New insights into
799 evolution of the subcontinental mantle: Ore Geology Reviews, 90, 210–225.
800 Matsumoto, T., Morishita, T., Masuda, J., Fujioka, T., Takebe, M., Yamamoto, K., Arai, S. (2005).
801 Noble gases in the Finero Phlogopite–Peridotites, ItalianWestern Alps. Earth and Planetary Science
802 Letters, 238, 130-145.
803 Matysiak, A.K., Trepmann, C.A. (2015). The deformation record of olivine in mylonitic peridotites
804 from the Finero Complex, Ivrea Zone: Separate deformation cycles during exhumation. Tectonics,
805 34, 2514-2533.
806 Mazzucchelli, M., Rivalenti, G., Piccirillo, E.M., Girardi, V.A.V., Civetta, L., Petrini, R. (1995).
807 Petrology of the Proterozoic mafic dyke swarms of Uruguay and constraints on their mantle source
808 composition.Precambrian Research, 74, 177-194.
809 Mazzucchelli, M., Rivalenti, G., Brunelli, D., Zanetti, A., Boari, E. (2009). Formation of highly
810 refractory dunite by focused percolation of pyroxenite-derived melt in the Balmuccia peridotite
811 Massif (Italy). Journal of Petrology, 50, 1205-1233.
812 Mazzucchelli, M., Zanetti, A., Rivalenti, G., Vannucci, R., Correia, C.T., Tassinari, C.C.G. (2010).
813 Age and geochemistry of mantle peridotites and diorite dykes from the Baldissero body: Insights
814 into the Paleozoic-Mesozoic evolution of the Southern Alps. Lithos, 119, 485-500.
815 Mazzucchelli, M., Quick, J.E., Sinigoi, S., Zanetti, A., Giovanardi, T. (2014). Igneous evolutions
816 across the Ivrea crustal section: The Permian Sesia Magmatic System and the Triassic Finero
817 intrusion and mantle. Geological Filed Trips, 6 (2.2), 1-98.

818 Mazzucchelli, M., Cipriani, A., Hémond, C., Zanetti, A., Bertotto, G.W., Cingolani, C.A. (2016).
819 Origin of the DUPAL anomaly in mantle xenoliths of Patagonia (Argentina) and geodynamic
820 consequences. Lithos, 248-251, 257-271.
821 McDonough, W.F., Sun, S.-s. (1995). The composition of the Earth. Chemical Geology, 120, 223-
822 253.
823 Milholland, C.S. & Presnall, D.C. (1998). Liquidus phase relations in the CaO-MgO-Al2O3-SiO2
824 system at 3.0 GPa: the Aluminous pyroxene thermal divide and high-pressure fractionation of
825 picritic and komatiitic magmas. Journal of Petrology, 39, 3-27.
826 Morishita, T., Arai, S., Tamura, A. (2003). Petrology of an apatite-rich layer in the Finero
827 phlogopite–peridotite, Italian Western Alps; implications for evolution of a metasomatising agent.
828 Lithos, 69, 37-49.
829 Morishita, T., Hattori, K.H., Terada, K., Matsumoto, T., Yamamoto, K., Takebe, M., Ishida, Y.,
830 Tamura, A., Arai, S. (2008). Geochemistry of apatite-rich layers in the Finero phlogopite–peridotite
831 massif (Italian Western Alps) and ion microprobe dating of apatite. Chemical Geology, 251, 99-
832 111.
833 Mukasa, S.B. & Shervais, J.W. (1999). Growth of subcontinental lithosphere: evidence from
834 repeated dike injections in the Balmuccia lherzolite massif, Italian Alps. Lithos 48, 287-316
835 Obermiller, W.A., 1994. Chemical and isotopic variations in the Balmuccia, Baldissero and Finero
836 peridotite massifs (Ivrea-Zone, N-Italy). Unpublished PhD thesis, Johannes Gutenberg-Universität
837 Mainz, pp. 191.
838 Perinelli, C., Armienti, P., Dallai, L. (2011). Thermal evolution of the lithosphere in a rift
839 environment as inferred from the geochemistry of mantle cumulates, Northen Victoria Land,
840 Antarctica. Journal of Petrology, 52, 665-690.
841 Petri, B., Duretza, T., Mohn, G., Schmalholz, S.M., Karner, G.D., Müntener, O. (2019). Thinning
842 mechanisms of heterogeneous continental lithosphere. Earth and Planetary Science Letters, 512,
843 147-162.

844 Piccardo, G.B., Zanetti, Z., Müntener, O. (2007). Melt/peridotite interaction in the Southern Lanzo
845 peridotite: field, textural and geochemical evidence. Lithos, 94, 181-209.
846 Polat, A., Frei, R.,. Longstaffe, F.J., Thorkelson, D.J., Friedman, E. (2018). Petrology and
847 geochemistry of the Tasse mantle xenoliths of the Canadian Cordillera: A record of Archean to
848 Quaternary mantle growth, metasomatism, removal, and melting. Tectonophysics, 737, 1-26.
849 Ponce, A.D., Bertotto, G.W., Zanetti, A., Brunelli, D., Giovanardi, T., Aragón, E., Bernardi, M.I.,
850 Hémond, C., Mazzucchelli, M. (2015). Short-scale variability of the SCLM beneath the extra-
851 Andean back-arc (Paso de Indios, Argentina): evidence fromspinel-facies mantle xenoliths. Open
852 Geosciences 7, 362–385.Quick, J.E., Sinigoi, S., Mayer, A. (1995). Emplacement of mantle
853 peridotite in the lower continental crust, Ivrea-Verbano Zone, northwest Italy. Geology, 23/8, 739-
854 742.
855 Princivalle, F., DeMin, A., Lenaz, D., Scarbolo, M., Zanetti, A. (2014). Ultramafic xenoliths from
856 Damaping (Hannuoba region, NE-China): Petrogenetic implications from crystal chemistry of
857 pyroxenes, olivine and Cr-spinel and trace element content of clinopyroxene. Lithos, 188, 3-14.
858 Quick, J.E., Sinigoi, S., Mayer, A. (1995). Emplacement of mantle peridotite in the lower
859 continental crust, Ivrea-Verbano Zone, northwest Italy. Geology, 23, 739-742.
860 Raffone, N., Le Fèvre, B. L., Ottolini, L., Vannucci, R., Zanetti, A. (2006). Light-lithophile element
861 metasomatism of Finero peridotite (W Alps): A secondary-ion mass spectrometry study.
862 Microchimica Acta, 155, 251-255.
863 Ridolfi, F., Zanetti, A., Renzulli, A., Perugini, D., Holtz, F., Oberti, R. (2018). AMFORM, a new
864 mass-based model for the calculation of the unit formula of amphiboles from electron microprobe
865 analyses. American Mineralogist, 103, 1112-1125.
866 Rivalenti, G., Mazzucchelli, M., Molesini, M., Petrini, R., Girardi, V.A.V., Bossi, J., Campal, N.
867 (1995). Petrology of late proterozoic mafic dikes in the Nico Perez region, central Uruguay.
868 Mineralogy and Petrology, 55, 239-263.

869 Rivalenti, G., Mazzucchelli, M., Zanetti, A., Vannucci, R., Bollinger, C., Hémond, C., Bertotto,
870 G.W. (2007a). Xenoliths from Cerro de los Chenques (Patagonia): An example of slab-related
871 metasomatism in the backarc lithospheric mantle, Lithos, 99, 45-67.
872 Rivalenti, G., Zanetti, A., Girardi, V.A.V., Mazzucchelli, M., Tassinari, C.C.G., Bertotto, G.W.
873 (2007b). The effect of the Fernando de Noronha plume on the mantle lithosphere in north-eastern
874 Brazil. Lithos, 94, 111-131.
875 Rocco, I., Zanetti, A., Melluso, L., Morra, V. (2017). Ancient-depleted and enriched mantle
876 lithosphere domains in northern Madagascar: geochemical and isotopic evidence from spinel-to-
877 plagioclase-bearing ultramafic xenoliths. Chemical Geology, 466, 70-85.
878 Rollinson, H. (1993). Using geochemical data: evaluation, presentation interpretation. Longman
879 Group UK Ltd, 1994 reprinted.
880 Sapienza, G.T., Scambelluri, M., Braga, R. (2009). Dolomite-bearing orogenic garnet peridotites
881 witness fluid-mediated carbonrecycling in a mantle wedge (Ulten Zone, Eastern Alps, Italy).
882 Contributions to Mineralogy and Petrology, 158, 401-420.
883 Sato, K., Miyamoto, T., Kawasaki, T. (2006). Experimental calibration of sapphirine-spinel Fe^{2+}-
884 Mg exchange thermometer: implication for constraints on P-T condition of Howard Hills, Napier
885 Complex, East Antarctica. Gondwana Research, 9, 398-408.
886 Schaltegger, U., Ulianov, A., Müntener, O., Ovtcharova, M., Peytcheva, I., Vonlanthen, P.,
887 Vennemann, T., Antognini, M., Girlanda, F. (2015). Megacrystic zircon with planar fractures in
888 miaskite–type nepheline pegmatites formed at high pressures in the lower crust (Ivrea Zone,
889 southern Alps, Switzerland). American Mineralogist 100, 83-94.
890 Schmid, S.M., Bernoulli, D., Fügenschuh, B., Matenco, L., Schefer, S., Schuster, R., Tischler, M.,
891 Ustaszewsk, K. (2008). The Alpine-Carpathian-Dinaridic orogenic system: correlation and
892 evolution of tectonic units. Swiss Journal of Geosciences, 101, 139-183.

893 Schulmann, K., Lexa, O., Janoušek, V., Lardeaux, J.M., Edel, J.B. (2014). Anatomy of a diffuse
894 cryptic suture zone: An example from the Bohemian Massif, European Variscides. Geology, 42,
895 275-278.
896 Selverstone, J. & Sharp, Z.D., (2011). Chlorine isotope evidence for multicomponent mantle
897 metasomatism in the Ivrea Zone. Earth and Planetary Science Letters, 310, 429-440.
898 Siena, F., & Coltorti, M. (1989). The petrogenesis of a hydrated mafic - ultramafic complex and the
899 role of amphibole fractionation at Finero (Italian Western Alps). Neues Jahrbuch für Mineralogie, 6,
900 255-274.
901 Sills, J.D., Ackermand, D., Herd, R.K., Windley, B.F. (1983). Bulk composition and mineral
902 parageneses of sapphirine-bearing rocks along a gabbro-lherzolite contact at Finero, Ivrea Zone, N
903 Italy. Journal of metamorphic Geology, 1, 337-351.
904 Stälhe, V., Frenzel, G., Kober, B., Michard, A., Puchelt, H., Schneider, W. (1990). Zircon syenite
905 pegmatites in the Finero peridotite (Ivrea Zone): evidence for a syenite from a mantle source. Earth
906 and Planetary Science Letters, 101, 196-205.
907 Stähle, V., Frenzel, G., Hess, J. C., Saupé, F., Schmidt, S. Th., Schneider, W. (2001). Permian
908 metabasalt and Triassic alkaline dykes in the Northern Ivrea Zone: clues to the post-Variscan
909 geodynamic evolution of the Southern Alps. Schweizerische Mineralogische und Petrographische
910 Mitteilungen, 81, 1-21.
911 Tiepolo, M., Oberti, R., Zanetti, A., Vannucci, R, Foley, S.F. (2007). Trace-Element partitioning
912 between Amphibole and silicate melt. Reviews in Mineralogy and Geochemistry, 67, 417-452.
913 Tommasi, A., Langone, A., Padrón-Navarta, J. A., Zanetti, A., Vauchez, A. (2017). Hydrous melts
914 weaken the mantle, crystallization of pargasite and phlogopite does not: Insights from a
915 petrostructural study of the Finero peridotites, Southern Alps. Earth and Planetary Science Letters,
916 477, 59–72.

917 Tribuzio, R., Renna, M., Dallai, L., Zanetti, A. (2014). The magmatic–hydrothermal transition in
918 the lower oceanic crust: Clues from the Ligurian ophiolites, Italy. Geochimica et Cosmochimica
919 Acta, 130, 188–211.
920 Workman, R.K., Hart, S.R. (2005). Major and trace element composition of the depleted MORB
921 mantle (DMM). Earth Planetary Science Letter, 231, 53–72.
922 Zanetti, A., Mazzucchelli, M., Rivalenti, G., Vannucci, R. (1999). The Finero phlogopite-peridotite
923 massif: an example of subduction-related metasomatism. Contributions to Mineralogy and
924 Petrology, 134, 107-122.
925 Zanetti, A., Mazzucchelli, M., Sinigoi, S., Giovanardi, T., Peressini, G., Fanning, M. (2013).
926 Insights into the Melt-Lower Crust Interplay in Subduction-related Setting and the Mesozoic
927 Geodynamic Evolution of the Southern Alps: evidence from the Finero Mafic Complex (Ivrea-
928 Verbano Zone). Journal of Petrology, 54, 2235-2265.
929 Zanetti, A., Mazzucchelli, M., Sinigoi, S., Giovanardi, T., Peressini, G., Fanning, M. (2014).
930 Erratum Insights into the Melt-Lower Crust Interplay in Subduction-related Setting and the
931 Mesozoic Geodynamic Evolution of the Southern Alps: evidence from the Finero Mafic Complex
932 (Ivrea-Verbano Zone). Journal of Petrology, 55, 1239-1240.
933 Zanetti, A., Giovanardi, T., Langone, A., Tiepolo, M., Wu, F.-Y., Dallai, L., Mazzucchelli, M.,
934 (2016). Origin and age of zircon-bearing chromitite layers from the Finero phlogopite peridotite
935 (Ivrea–Verbano Zone, Western Alps) and geodynamic consequences. Lithos, 262, 58-74.
936

937 **Figure captions**

938 Figure 1: geological map of the Finero area, modified after Mazzucchelli et al. (2014).

939

940 Figure 2: A) sample FI09C06 crosscutting the host harzburgite foliation. The centre of the dyke is
941 formed by the Leucocratic Zone, while the melanocratic zones (i.e. Opx Zone, Early Amph Zone
942 and Late Amph Zone) are indistinguishable; B) phlogopite vein cutting the Opx Zone; C-F)

943 occurrences of sapphirine in sample FI09C06 (C and D) and sample FI9664 (E and F). The figures
944 show the increase of sapphirine size, from μm (C) to millimeter (D and E) up to centimeter (F).
945
946 Figure 3: PM primitive mantle-normalized bulk rock trace element patterns of gabbroic dyke and
947 host harzburgite. PM values are from McDonough and Sun (1995). Literature values from the
948 harzburgite-pyroxenite association from (1) Hartmann and Wedephol (1993) and from nepheline-
949 bearing hornblende syenitic dykes from (2) Stähle et al. (2001) are reported for comparison.
950
951 Figure 4: Orthopyroxene major element contents from host harzburgites, dykes and literature data.
952 Plotted literature data are: harzburgite-pyroxenite association orthopyroxene from (1) Zanetti et al.
953 (1999) and orthopyroxene from sapphirine-bearing rock from the Mafic Complex from (2) Sills et
954 al. (1983).
955
956 Figure 5: Phlogopite major element contents from host harzburgites, dykes and literature data.
957 Plotted literature data are: harzburgite-pyroxenite association phlogopite from (1) Zanetti et al.
958 (1999).
959
960 Figure 6: Amphibole major element contents from host harzburgites, dykes and literature data.
961 Plotted literature data are: harzburgite-pyroxenite association amphibole compositions from (1)
962 Zanetti et al. (1999) and (2) Morishita et al. (2008), amphibole from Ap-rich veins from FPP from
963 (1) Zanetti et al. (1999) and (2) Morishita et al. (2008) and amphibole from sapphirine-bearing rock
964 from the Mafic Complex from (3) Sills et al. (1983).
965
966 Figure 7: Sapphirine compositions plotted in the (MgO+FeO)-(Cr2O3+Fe2O3+Al2O3)-SiO2
967 diagram (mol. %). Literature data are from sapphirine from the Finero Mafic Complex (Sills et al.,
968 1983) and from sapphirine 1 from Higgins et al. (1979).

969

970 Figure 8: REE patterns of clinopyroxene and amphibole from the gabbroic dykes and the
971 respectively host rocks divided for samples and position. Values are normalized to Chrondrite-I (CI,
972 values from Lyubetskaya and Korenaga (2007). $\delta^{18}O$ values (normalized to SMOW) from phases of
973 sample FI09C06 are reported near the REE patterns according to their position in the sample.

974

975 Figure 9: PM primitive mantle-normalized trace element patterns of clinopyroxene from host
976 harzburgite. PM values are from McDonough and Sun (1995). Plotted literature data are:
977 clinopyroxene and amphibole average compositions from harzburgite-pyroxenite association from
978 (1) Zanetti et al. (1999) and (2) Morishita et al. (2008), clinopyroxene and amphibole average from
979 Ap-rich veins from FPP from (1) Zanetti et al. (1999) and (2) Morishita et al. (2008) reported as
980 Ap-veins.

981

982 Figure 10: PM primitive mantle-normalized trace element patterns of amphiboles from gabbroic
983 dyke and host harzburgite. PM values are from McDonough and Sun (1995).

984

985 Figure 11: $\delta^{18}O$ normalized to SMOW. From literature are reported the field of mantle and variation
986 of MORB from Rollinson (1993), mantle ultramafics and mantle-derived melts from (*) Bindeman
987 (2008). Finero literature data are reported from harzburgite-pyroxenite association from Hartmann
988 and Wedephol (1993) and Selverstone and Sharp (2011) and from chromitite in dunite bodies from
989 Zanetti et al. (2016).

990

991 Figure 12: $^{143}Nd/^{144}Nd$ vs $^{87}Sr/^{86}Sr$ recalculated at 225 Ma of Amph and Plg from the various zone
992 of FI09C06 sample (host and dyke). (1) Amph data of FPP from Obermiller (1994); (2) bulk rock of
993 the Finero Mafic Complex from Lu et al. (1997b); (3) Alkaline dyke in FPP from Stähle et al.
994 (1990); (4) Alkaline dyke in FPP from Stähle et al. (2001); (5) Mesozoic shoshonitic magmatism

995 (SS: Silica-Saturated; US: Undersaturated-Silica) in the Predazzo area from Casetta et al. (2018);
996 DMM from Workman and Hart (2005). Mixing model was calculated between the two end-
997 members the alkaline dyke S9 of Stähle et al. (1990) and the hosting peridotite FI09C06. Data for
998 the melt in equilibrium with the alkaline dyke S9 are: $^{143}Nd/^{144}Nd$ = 0.512607, $^{87}Sr/^{86}Sr$ = 0.703720
999 (from Stähle et al., 1990; recalculated at 225Ma), Nd = 8.333 ppm and Sr = 830 ppm (calculated
1000 from LA-ICP-MS Plg analysis of albitite dykes similar to the dyke of Stähle et al., 1990, using the
1001 K_d of Dohmen and Blundy, 2014; average Nd = 0.25 ppm, Sr = 5810 ppm). Data for the melt in
1002 equilibrium with the host FPP peridotite are $^{143}Nd/^{144}Nd$ = 0.512130, $^{87}Sr/^{86}Sr$ = 0.708501
1003 (recalculated at 225Ma), Nd = 67.5 ppm and Sr = 909 ppm (calculated using the K_d of Ionov et al.,
1004 2002).

Figure 1

Click here to download high resolution image

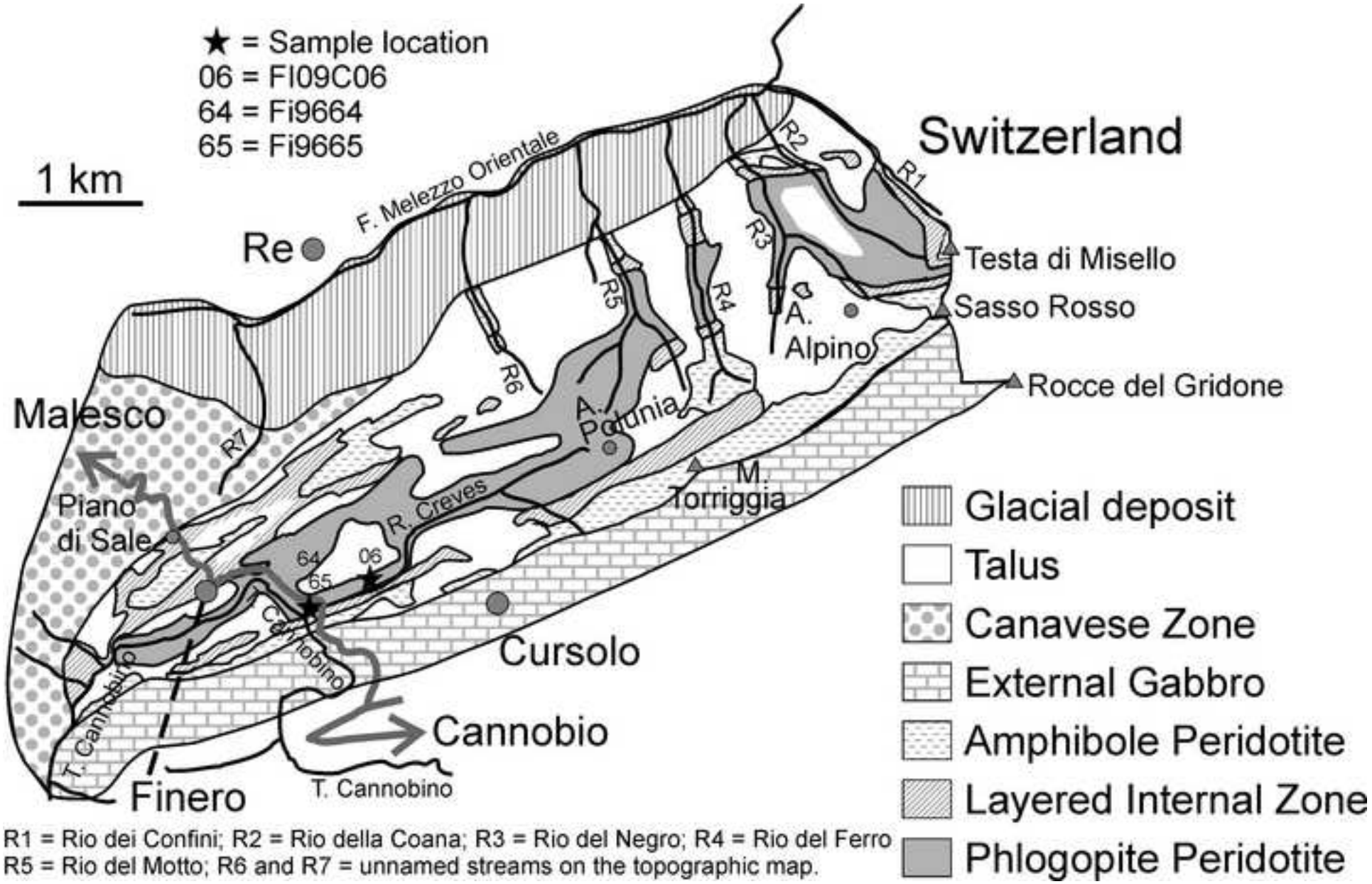

R1 = Rio dei Confini; R2 = Rio della Coana; R3 = Rio del Negro; R4 = Rio del Ferro
R5 = Rio del Motto; R6 and R7 = unnamed streams on the topographic map.

Figure 2

Click here to download high resolution image

Figure 3

Click here to download high resolution image

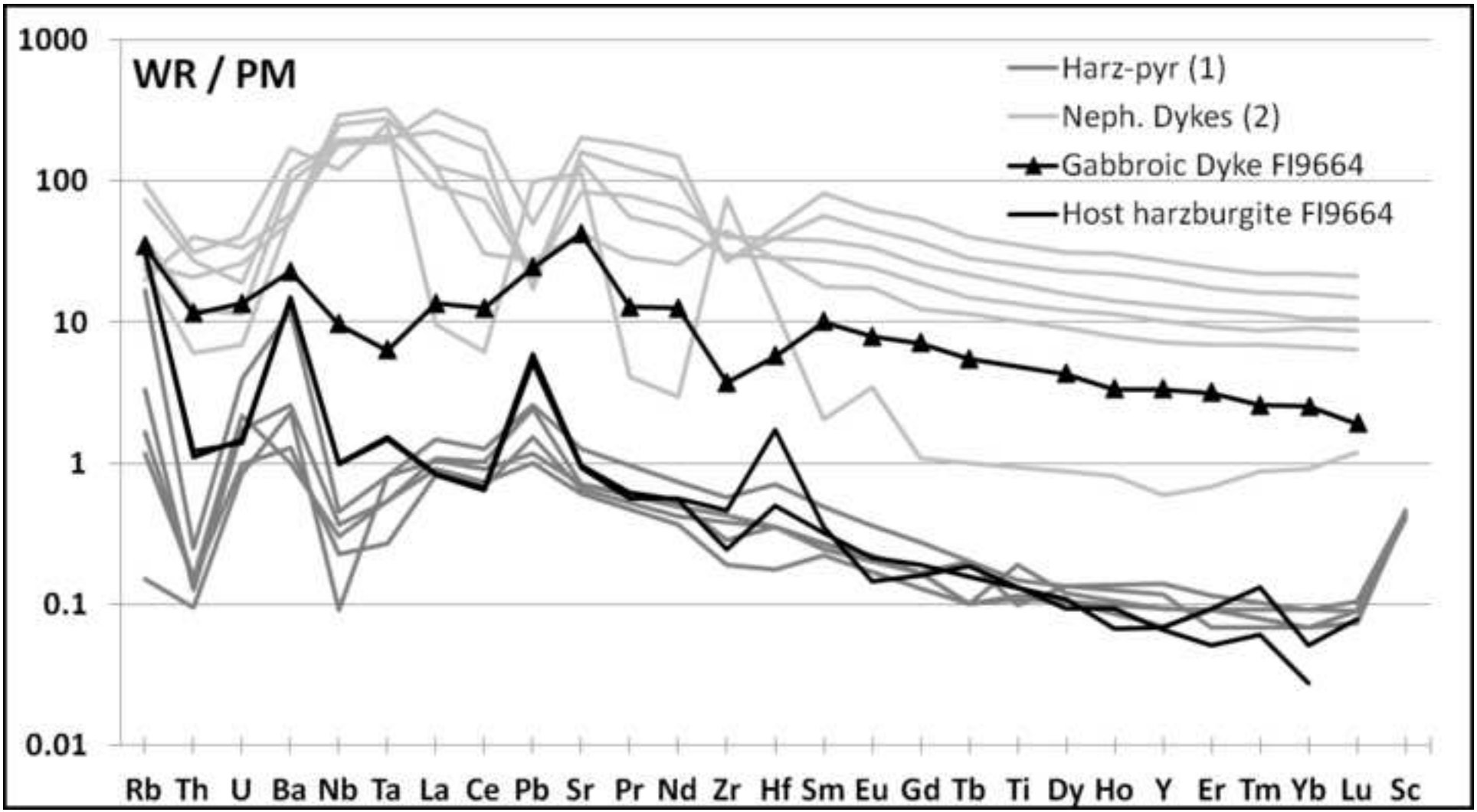

Figure 4

Click here to download high resolution image

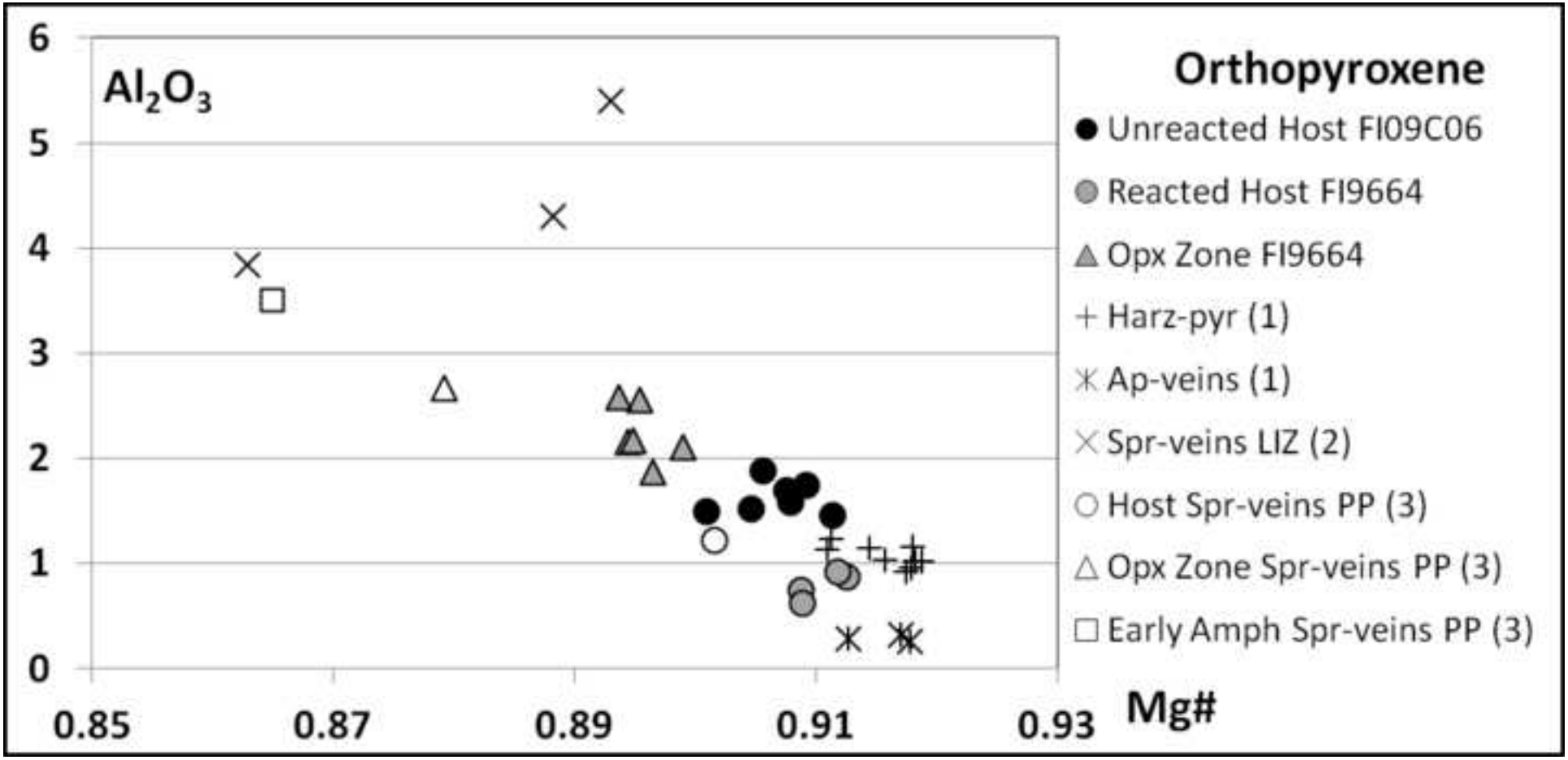

Figure 5

Click here to download high resolution image

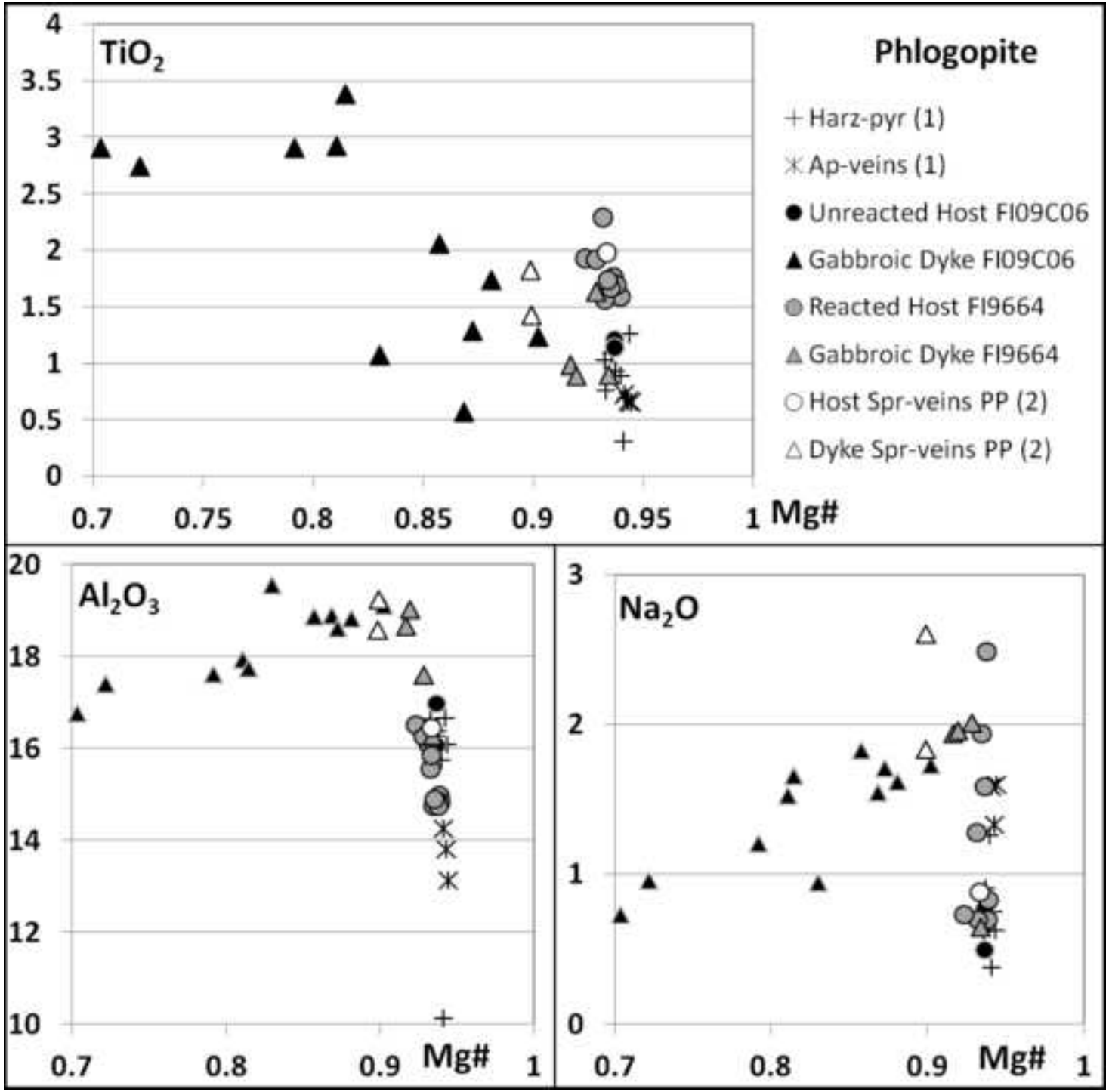

Figure 6

Click here to download high resolution image

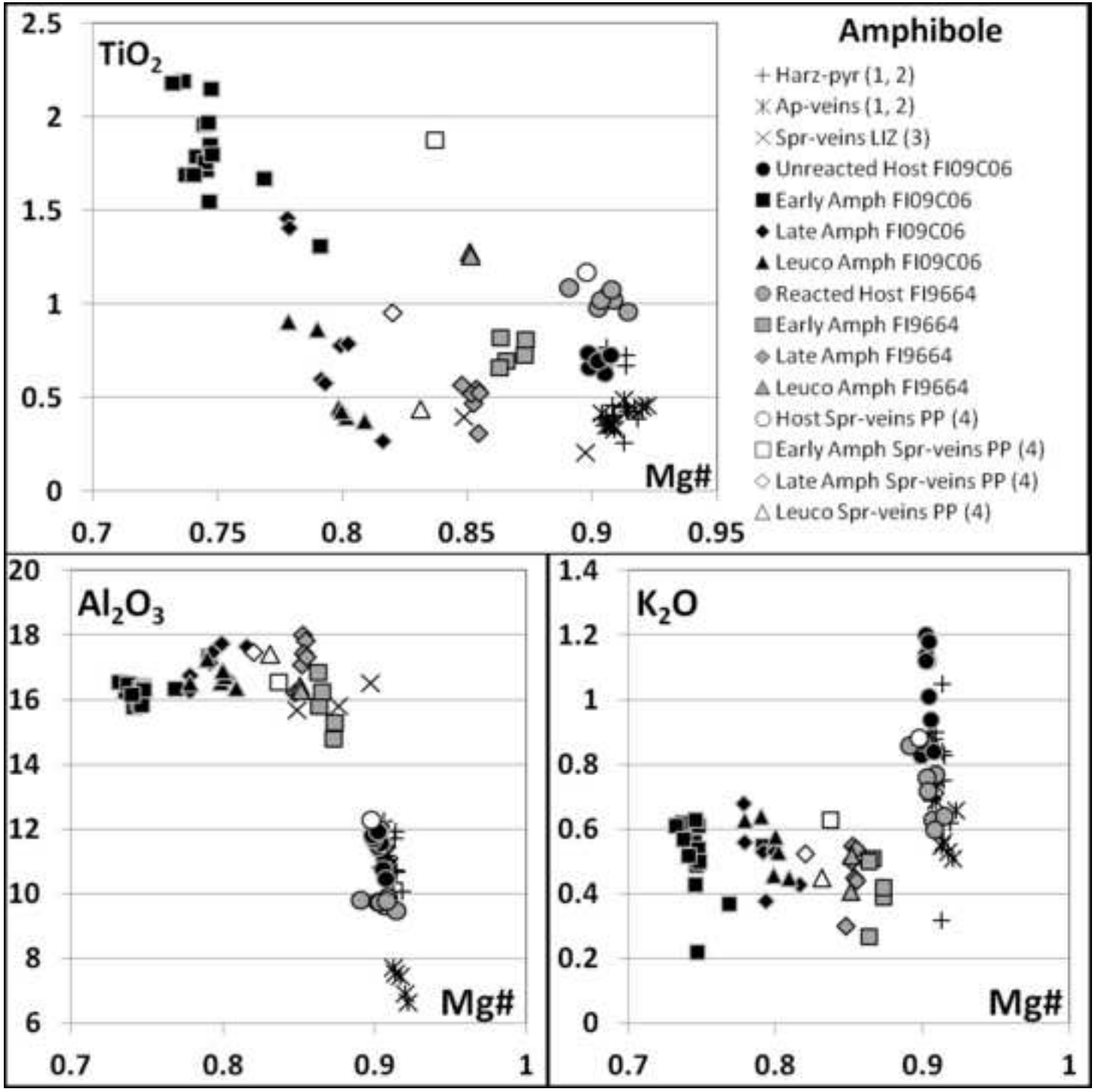

Figure 7

Click here to download high resolution image

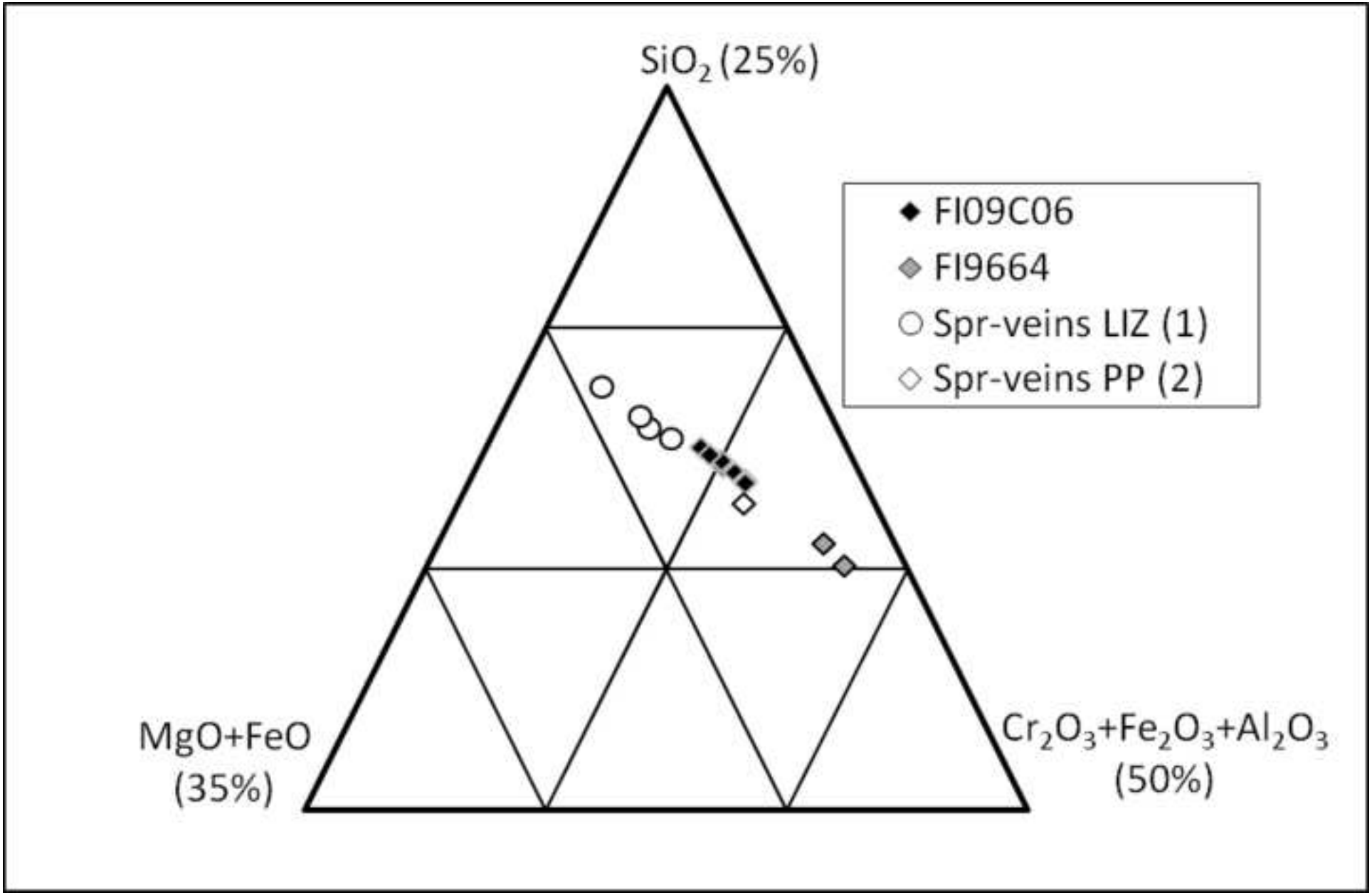

Figure 8

Click here to download high resolution image

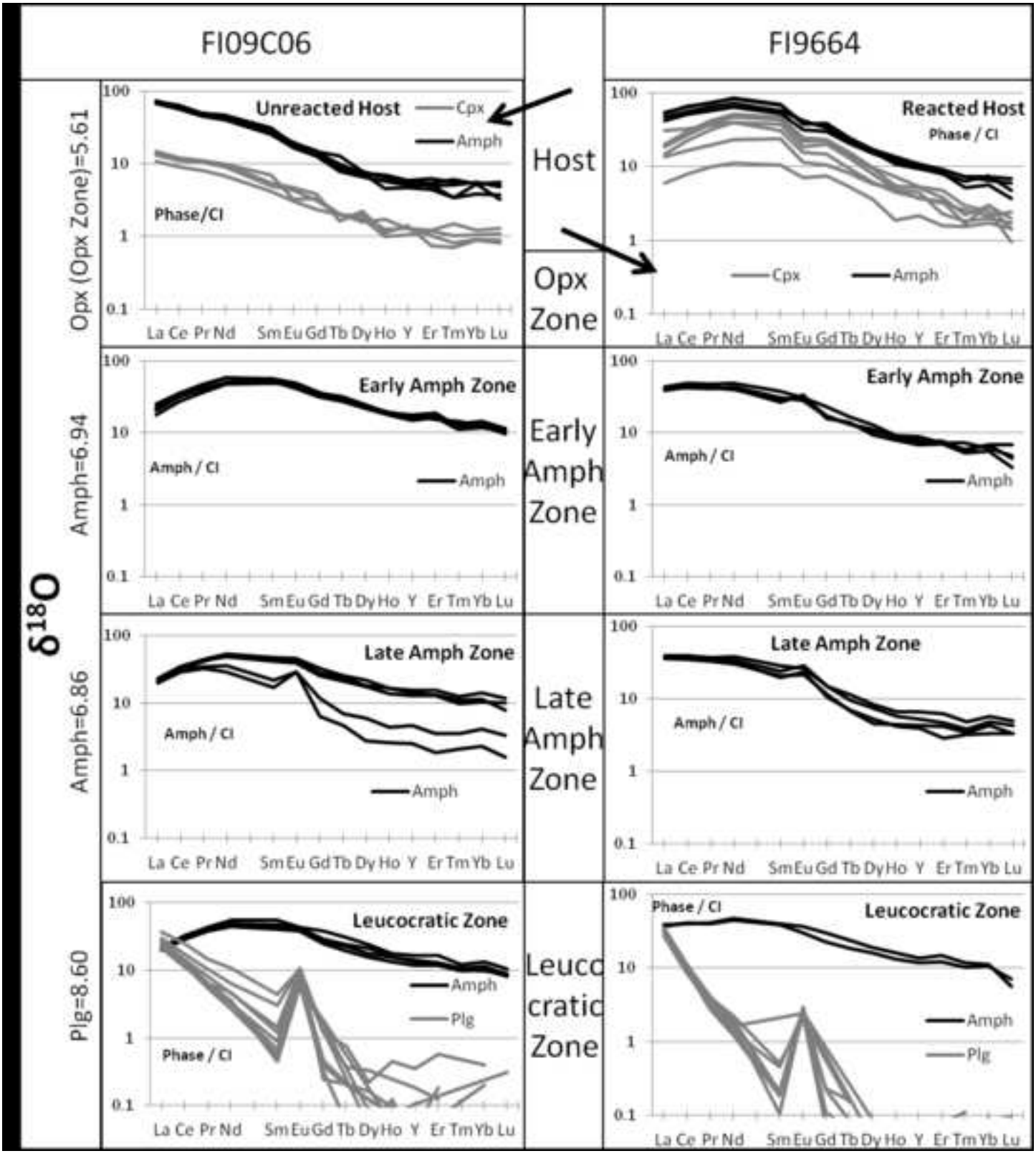

Figure 9

Click here to download high resolution image

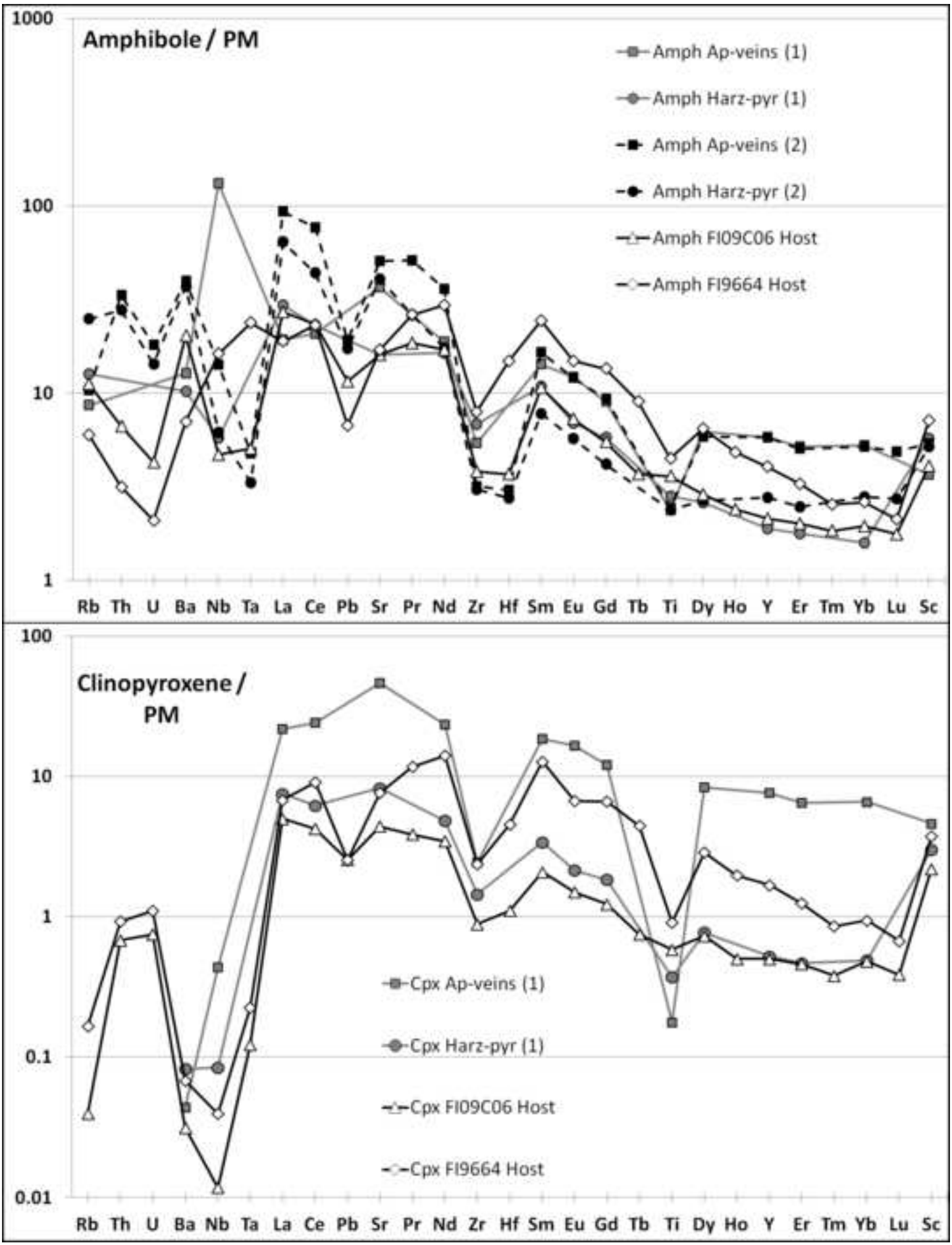

Figure 10

Click here to download high resolution image

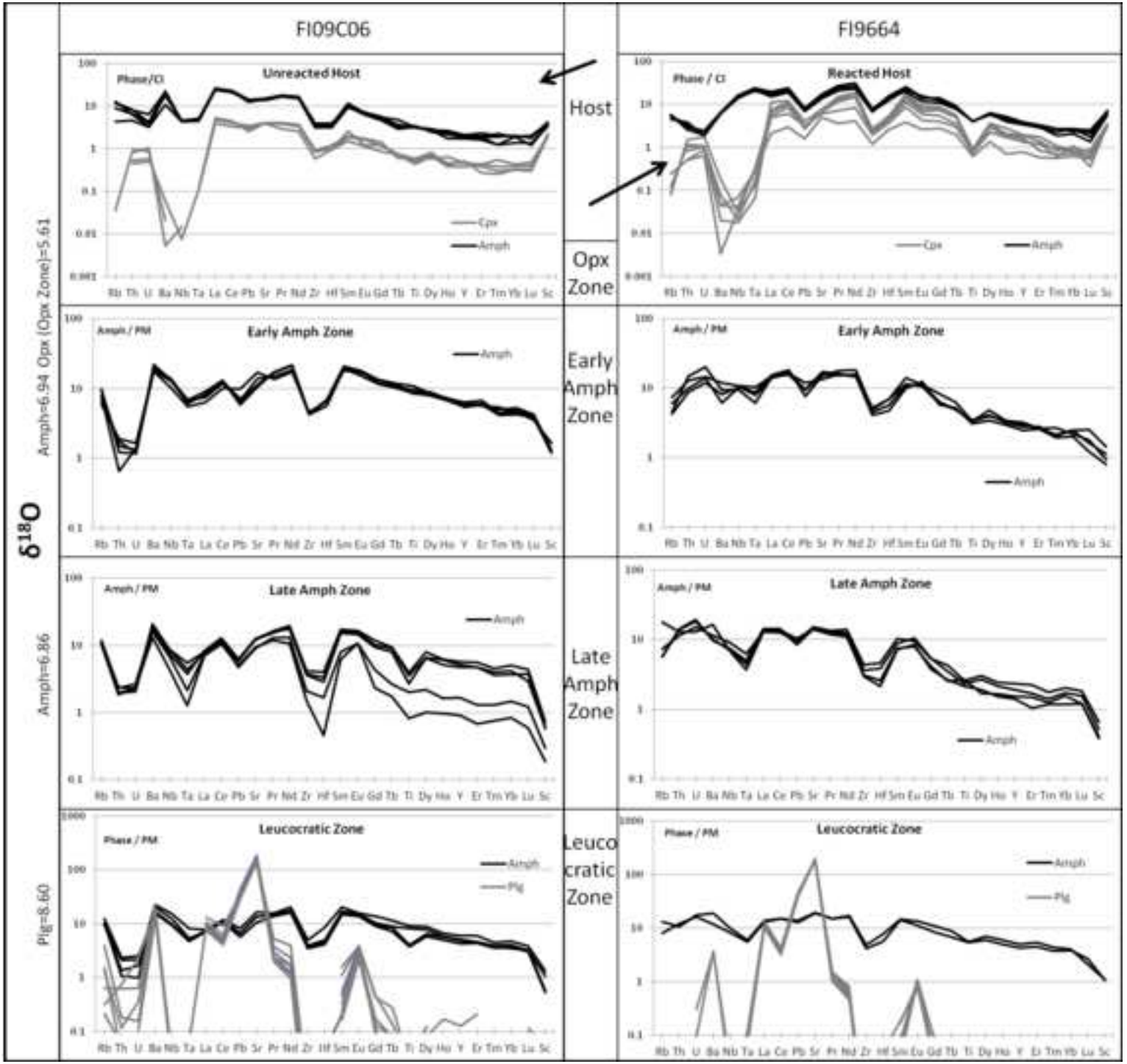

Figure 11

Click here to download high resolution image

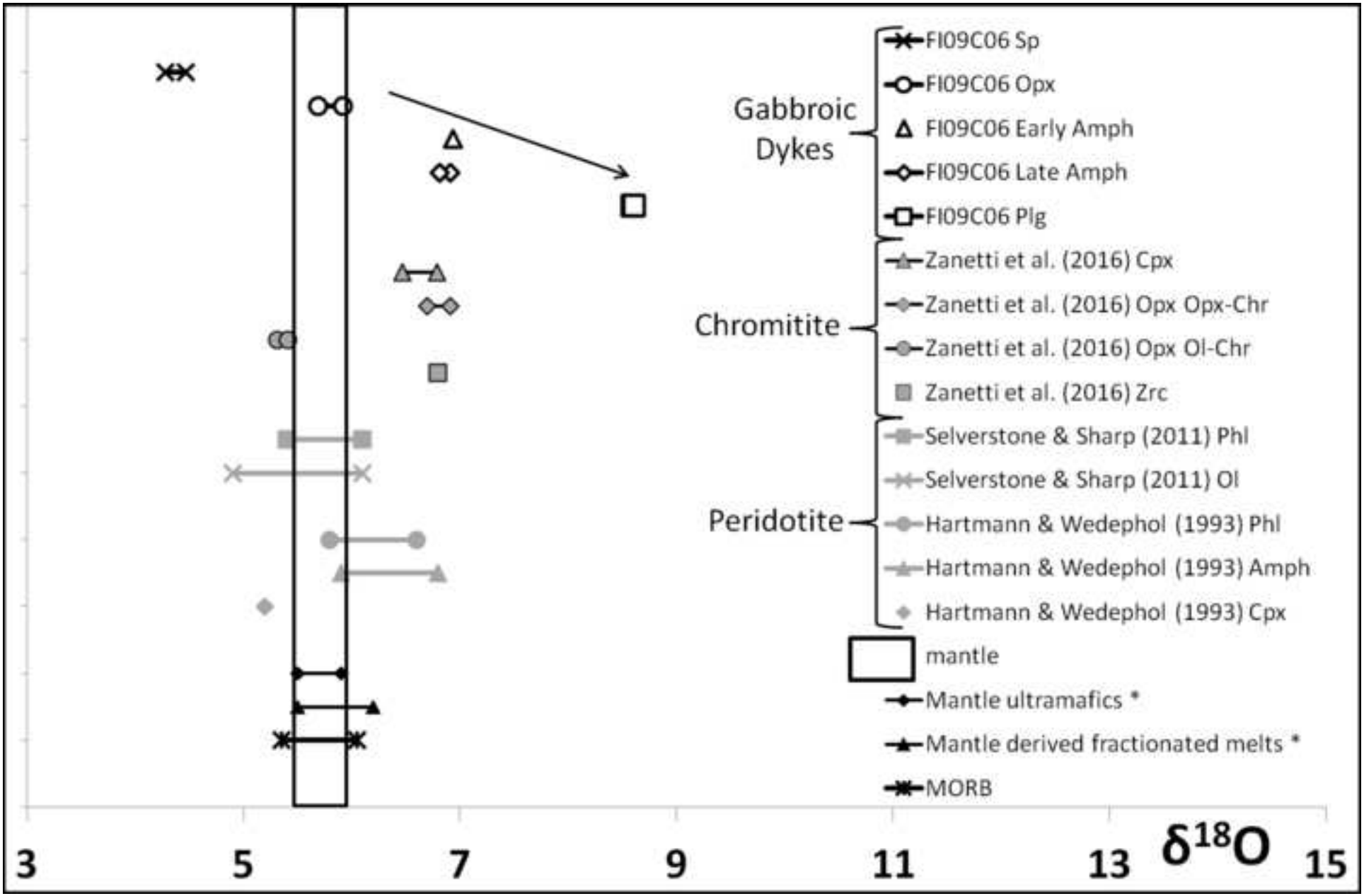

Figure 12

Click here to download high resolution image

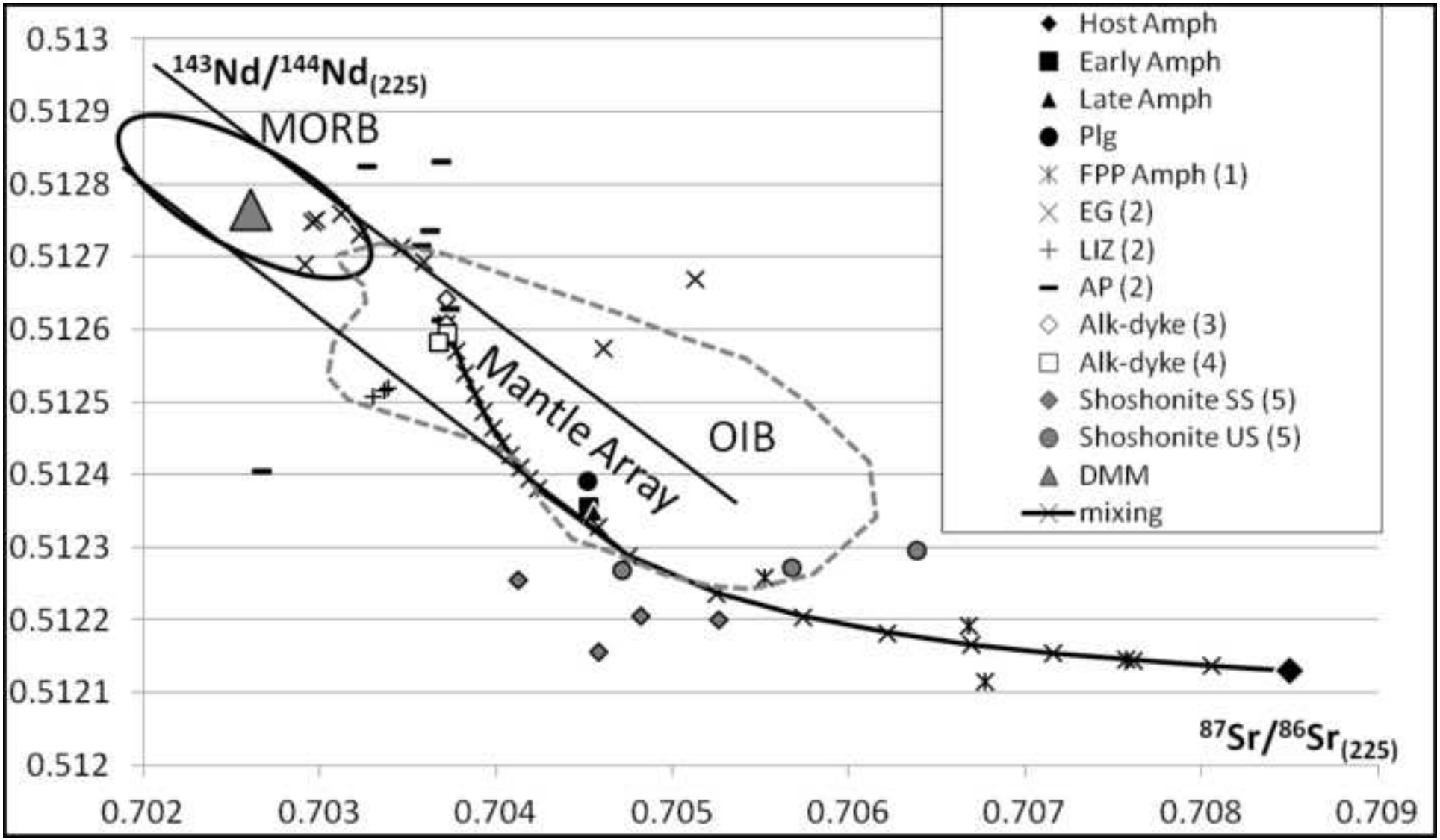

Table 1

Click here to download Table: Table 1.docx

Table 1: O isotopic composition of minerals from the Spr-bearing gabbroic dykes.

Sample	**Phase**	**$\delta^{18}O$**	**std. dev.**
FI09C06	Early Amph	6.94	0.00
FI09C06	Late Amph	6.86	0.05
FI09C06	Plg	8.60	0.01
FI09C06	Opx	5.81	0.11

Table 2

Click here to download Table: Table 2.docx

Table 2: Sr and Nd isotopic composition of minerals from sample FI09C06 from the Spr-bearing gabbroic dykes and the host peridotite.

Rock	Phase	Rb	Sr	$^{87}Sr/^{86}Sr$	2SE	$^{87}Rb/^{86}Sr$	Nd	Sm	$^{143}Nd/^{144}Nd$	2SE	$^{147}Sm/^{144}Nd$
Host	Amph	6.5	281.2	0.708713	0.000008	0.066372	19.7	4.2	0.512317	0.000008	0.126796
Dyke	Early Amph	6.8	324.4	0.704722	0.000008	0.060834	24.8	8.1	0.512646	0.000008	0.197559
Dyke	Late Amph	8.6	189.5	0.704971	0.000008	0.131167	16.8	4.0	0.512559	0.000006	0.142593
Dyke	Plg	0.6	3109.7	0.704519	0.000008	0.000568	2.2	0.2	0.512482	0.000006	0.061238

Supplementary material A

Click here to download Background dataset for online publication only: Supplementary_material_A.xlsx

Supplementary material B

Click here to download Background dataset for online publication only: Supplementary_material_B.pdf

Supplementary material C

Click here to download Background dataset for online publication only: Supplementary_material_C.pdf